INTERNATIONAL JOURNAL OF REFRIGERATION 33 (2010) 1229–1250

available at www.sciencedirect.com

ScienceDirect

journal homepage: www.elsevier.com/locate/ijrefrig

Nucleate pool boiling, film boiling and single-phase free convection at pressures up to the critical state. Part I: Integral heat transfer for horizontal copper cylinders

Dieter Gorenflo, Elmar Baumhögger, Thorsten Windmann, Gerhard Herres*

Institut für Energie- und Verfahrenstechnik, Universität Paderborn, Warburger Str. 100, D-33098 Paderborn, Germany

Dedicated to Professor Dr.-Ing. Dr.h.c.mult. Karl Stephan on the occasion of his 80th birthday.

ARTICLE INFO

Article history:
Received 28 June 2010
Received in revised form
13 July 2010
Accepted 15 July 2010
Available online 22 July 2010

Keywords:
Heat transfer
Nucleate boiling
Film boiling
Critical heat flux
Free convection
Critical state

ABSTRACT

Transcritical working cycles for refrigerants have led to increased interest in heat transfer near the Critical State. In general, experimental results for this region differ significantly from those far from it because some fluid properties vary much more there than at a greater distance. In this paper, measurements for two-phase and single-phase free convective heat transfer from an electrically heated copper tube with 25 mm O.D. to refrigerant R125 are discussed for fluid states very close to the Critical Point and far from it. It is shown that heat transfer for film boiling slightly below and for free convection slightly above the critical pressure is very similar. The new – and also previous – experimental data for nucleate boiling, film boiling, and single-phase free convection are compared with calculated results between atmospheric and critical pressure. It can be concluded that the Principle of Corresponding States in its simplest form is very well suited to transfer the results to other refrigerants.

In Part II, particular attention will be given to a minimum superheat for nucleate boiling and a maximum superheat for film boiling and single-phase free convection within the circumferential variation of the isobaric wall superheat on the lower parts of the tube.

Ebullition libre nucléée, ébullition pelliculaire et convection libre monophasique à des pressions allant jusqu'à l'état critique. Partie I : transfert de chaleur intégral des cylindres horizontaux en cuivre

Mots clés : Transfert de chaleur ; Ébullition libre nucléée ; Ébullition pelliculaire ; Flux critique ; Convection libre ; État critique

* *Corresponding author*. Tel.: +49 5251 60 2393; fax: +49 5251 60 3522.
E-mail address: digo@thet.upb.de (D. Gorenflo).

0140-7007/$ – see front matter © 2010 Elsevier Ltd and IIR.
doi:10.1016/j.ijrefrig.2010.07.015

Nomenclature

A	surface area (m^2) of the tube
CP	Critical Point
h	specific enthalpy ($J\ kg^{-1}$)
Nu, Gr, Pr,	Nusselt, Grashof, Prandtl numbers (–)
p	pressure (bar)
p^*, ρ^*, T^*, v^*	reduced properties
Q	electrical energy input (W)
q	heat flux ($W\ m^{-2}$ or $kW\ m^{-2}$)
q_{max}	maximum heat flux ($kW\ m^{-2}$)
q_{min}	minimum heat flux ($kW\ m^{-2}$)
r	radius (m of bubble)
R_a	mean roughness height (μm), ISO 4287
T	temperature (K or °C)
α	heat transfer coefficient ($kW\ m^{-2}\ K^{-1}$)
ε	parameter for asymmetric variation of properties along ΔT (–)
φ	circumferential angle (°)
ρ	density ($kg\ m^{-3}$)
$(\delta\rho/\delta T)_p$	density gradient ($kg\ m^{-3}\ K^{-1}$)
$(\Delta\rho/\Delta T)_p$	density gradient for boundary layer ($kg\ m^{-3}\ K^{-1}$)
σ	surface tension ($N\ m^{-1}$)

Indices

B	reference value
c	at Critical Point
f	fluid state in the pool (far from test tube)
l	liquid
sat	at (vapour/liquid) saturation conditions
v	vapour
w	on wall of test tube

1. Introduction

Transcritical working cycles for refrigerants have led to increased interest in heat transfer near the Critical State in recent years. Experimental results for this region differ significantly from those far from it because some fluid properties (e.g. density or specific enthalpy) which are important for this kind of heat transfer, vary much more near the critical state than at a greater distance, if compared at a given isobaric driving temperature difference.

Forced convection is mainly used in this range in practice. It is not very convenient, however, to demonstrate the influence of the fluid properties that vary within the superheated boundary layer near the heated wall, since the bulk fluid state also varies in the downstream direction along the heat transfer area. Therefore, the configuration of a pool of fluid (thermostatted at exactly constant temperature) and a horizontal tube (with outer diameter not too small) are much more appropriate for this purpose. In addition, forced convection will always be accompanied by free convection in terrestrial gravity, if density varies as drastically with temperature as it does in the critical region.

Heat transfer measurements from an electrically heated copper tube with 25 mm O.D. to refrigerant R125($CHF_2.CF_3$) which is suitable in temperature and pressure for our test loop, are discussed for fluid states very close to the Critical Point (CP) and at a greater distance, for a wide range of heat fluxes. In particular, film boiling slightly below and (single-phase) free convection slightly above the critical pressure are compared.

The new experimental data ranging down to near-atmospheric pressures are also compared with calculated results for nucleate boiling, film boiling and single-phase free

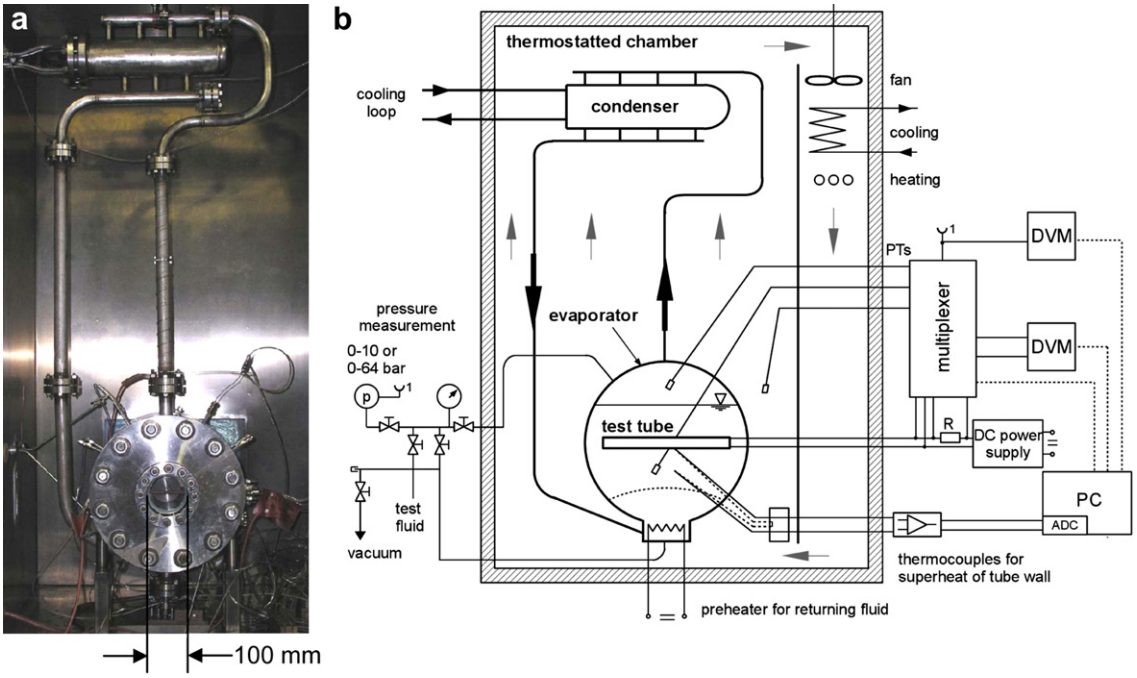

Fig. 1 – (a) Photo of test loop (without insulation); (b) Schematic representation of experimental apparatus.

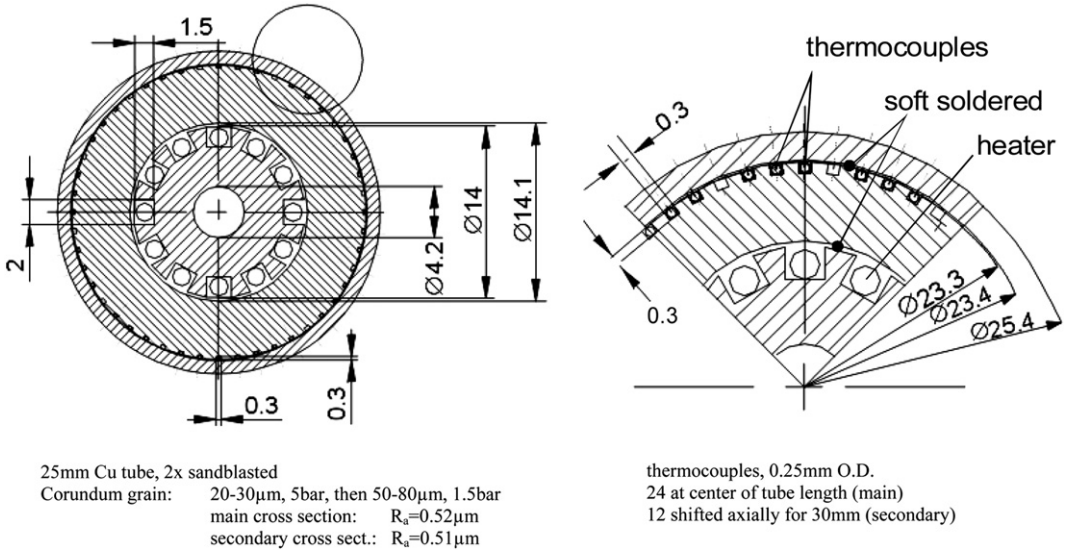

Fig. 2 – Cross section and detail of test tube, to scale.

convection, and with previous measurements for some refrigerants that have become outdated. It is shown that the Principle of Corresponding States in its simplest form is very well suited to transfer the results to other refrigerants.

In Part II of the paper, the circumferential variation of the wall superheat will be analyzed and related to the motion of the fluid within the superheated boundary layer and to the particular shape of the two-phase boundary between vapour and liquid near the heated wall, with a minimum in the wall superheat that develops or disappears under certain conditions on the lower parts of the wall for nucleate boiling, and with a maximum wall superheat for film boiling and single-phase free convection. These are interpreted using photographs of bubble formation or the existence of a wavy structure of the boundary layer, respectively.

2. Experimental equipment and procedure

The test loop mounted in a thermostatted chamber is shown in Fig. 1 on the left and the entire experimental equipment is represented schematically on the right. The test fluid is heated in the evaporator, it rises to the condenser where the heat is removed, and the fluid returns to the evaporator in natural convection. At pressures below critical, heat transfer is combined with vapour/liquid phase transition, and above critical, circulation is caused by the density difference between fluid states at higher or lower temperatures, respectively.

The heating element is a horizontal copper tube with 25 mm O.D. the surface of which had been sandblasted twice by Corundum grain with small particle size and high blasting pressure, then with coarser particles and lower pressure, see Fig. 2. In two cross sections (30 mm axial distance in between), the tube contains miniaturized thermocouples of 0.25 mm O.D., equally distributed along the circumference (24 in the 'main', and 12 in the 'secondary' cross section). Throughout the paper, the data points for the two cross sections are characterized in the new measurements by big (main) or small (secondary) symbols, see e.g. the upper diagram of Fig. 3.

The superheat of the tube surface, ΔT, used in the definition of the heat transfer coefficient α,

$$\alpha = \frac{q}{\Delta T} = \frac{Q}{A(T_w - T_f)}, \quad (1)$$

is measured directly, with *each* of the thermocouples having a reference junction in the fluid (40 mm below the tube) and a separate amplifier (a detailed analysis of the measuring techniques is given in Part II). The heat flux q is calculated from the (stabilized d_c-) electrical energy input Q and the tube surface area A. The experimental ΔT-values are corrected for heat conduction within the tube to the surface assuming *purely radial* heat flow (the consequences of this simplification will be discussed in Part II).

Measuring runs are always taken at constant pressure by precisely adjusting the heat removal from the cooling loop to the heat input at the test tube, and by thermostatting the temperature in the chamber to the equilibrium value belonging to the pressure chosen for the run. As a result, temperature and pressure vary by less than ±5 mK and ±5 mbar during each run.

3. Nucleate boiling

3.1. *New experimental data*

The new experimental data for nucleate boiling of R125 – ranging down to near-atmospheric pressures ($p_{min} = p^* \cdot p_c = 0.055 \cdot 36.177 = 1.99$ bar; p_c = critical pressure) – are represented in the double logarithmic plot of heat flux q over the superheat ΔT in the upper diagram of Fig. 3. The steep interpolation lines at constant pressure, characteristic of nucleate boiling, are shifted to smaller superheats with increasing pressure and start from single-phase turbulent free convection at the lowest pressure investigated, with

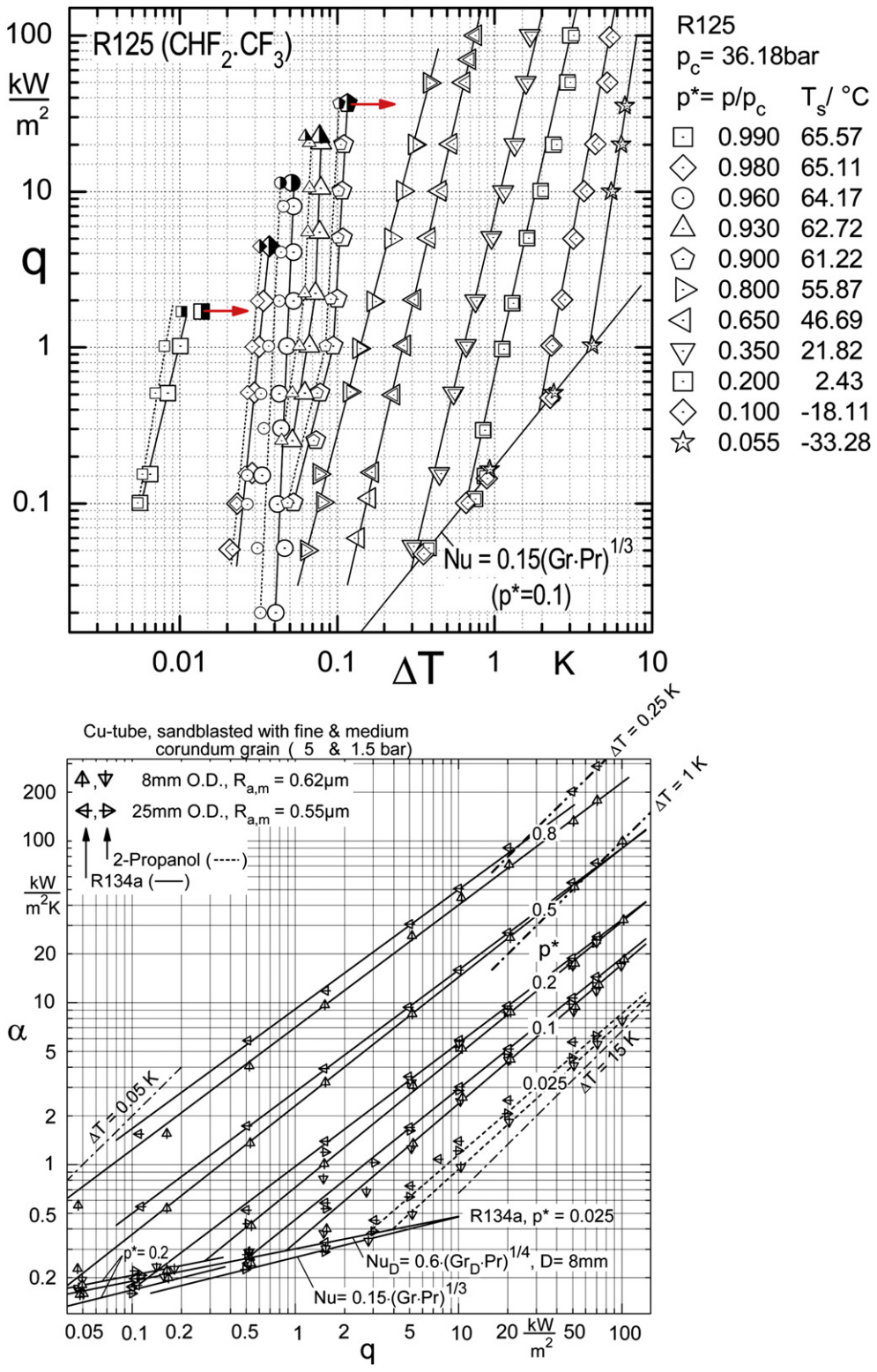

Fig. 3 – Top: Log,log $q(\Delta T)$-representation of the new results for nucleate boiling heat transfer from a horizontal 25 mm Cu tube with twice sandblasted surface to refrigerant R125. Bottom: Former measurements for R134a and 2-Propanol boiling on the 25 mm tube and an 8 mm tube with the same surface treatment as above (from Kotthoff and Gorenflo, 2009, modified).

$$Nu = 0.15(Gr\cdot Pr)^{0.33} \quad (2a)$$

The lower diagram shows for comparison earlier data for 2-Propanol and R134a starting from laminar free convection with

$$Nu_D = 0.60(Gr_D\cdot Pr)^{0.25} \quad (2b)$$

(*Nu*, *Gr*, *Pr* = Nusselt, Grashof and Prandtl numbers, respectively).

The steep increase in the upper diagram is particularly pronounced at very high reduced pressures $p^* \geq 0.9$ because the tube surface contains many similar, tiny cavities formed by

sandblasting with fine grain and high blasting pressure. At high p^*, these cavities are activated for bubble formation already at very small superheats because surface tension is very small near the Critical Point, and from Thomson's equation

$$\Delta p = 2\frac{\sigma}{r} \tag{3}$$

(here in its simplified form), the same follows for the excess pressure Δp which is related to ΔT, and which is necessary at equilibrium conditions inside a spherical bubble of radius r or a vapour nucleus existing within one of the cavities.

A more detailed examination of the runs at $p^* = 0.90–0.96$ in Fig. 3(top) reveals that for an increase in q of an order of magnitude or more ($1 \le q \le 10$ kW/m^2), ΔT increases only by 0.01–0.02 K. It is deduced that a great number of tiny cavities with almost the same size and shape exist within the roughness pattern of the heating surface, which become active nucleation sites at almost the same superheat ΔT when q is rising (at p = const) and which had been produced during the 1st blasting run with fine grain (narrow size distribution of 20–30 μm and high blasting pressure of 5 bar).

The same effect had been found earlier for this tube and another with 8 mm O.D. after sandblasting with the same corundum grain and the same blasting pressure, see the data points at $\Delta T = 0.25$ K ($p^* = 0.8$, $q \ge 50$ kW/m^2) and $\Delta T = 1.0$ K ($p^* = 0.5$, $q \ge 50$ kW/m^2) in the lower diagram of Fig. 3 (dot-dashed bold lines; from Kotthoff and Gorenflo, 2009).

The results indicate – together with Eq. (3) – that the many tiny cavities of the same size existing also there had been activated, because ΔT is greater by the same factor as surface tension σ, both compared to the data for $p^* = 0.9$ in the upper diagram (factors in ΔT: approximately 2.5 and 10; factors in σ: 2.57 and 10.2 for R134a at $p^* = 0.8$ & 0.5 compared to R125 at $p^* = 0.9$).

A further prerequisite for this effect is that the size of the bubbles leaving the heated surface, and their acceleration are also very small to avoid disturbance of the hydrodynamic and thermal conditions of neighbouring nucleation sites. This is also given at high reduced pressures as can be seen from the photo in Fig. 4 (Gorenflo et al., 2009; cf. also: Baumhögger et al., 2008) that was taken at $p^* = 0.9$, focussing at the plane containing the highest axial line of the tube surface (cf. also photos for the same pressure and higher q-values and for $p^* = 0.8$ in Part II).

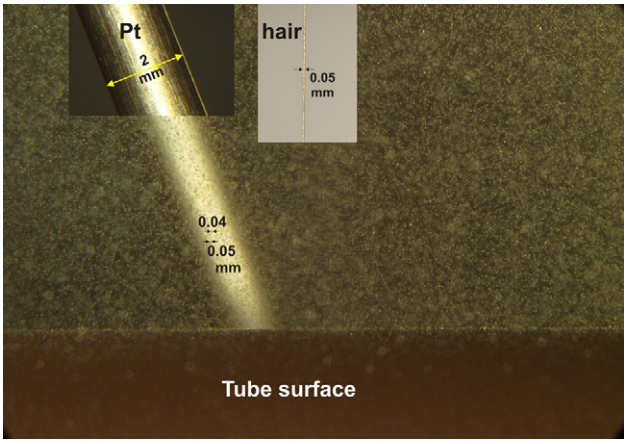

Fig. 4 – Photo of bubble formation at $p^* = 0.9$, $q = 20$ W/m^2; camera focussed at plane containing the highest axial line of the tube. For comparison: hair with 0.05 mm O.D.

By comparison with the inserted hair (of one of the authors), it follows that most of the bubble departure diameters are smaller than approximately 10 microns – the two bubbles of 40 and 50 microns identified in front of the 2 mm-PT resistance thermometer belong to the "biggest" that could be found among the bubbles originating from the top region of the tube. The rising velocity is very small for bubbles of this size and the comparatively small density differences between vapour and liquid at high reduced pressures.

3.2. *Comparison with calculated and former experimental data*

In the $\alpha(q)$-plots of Fig. 5, the new experimental results of Fig. 3 (symbols in the upper diagram) are compared with previous measurements for R115 boiling at equally high reduced pressures on two horizontal 8 mm copper tubes with emeried or commercially drawn surface, respectively (symbols in the lower diagram; Wickenhäuser, 1972; Bier et al., 1977a) and with the updated VDI-Heat Atlas calculation method (dot-dashed lines; Gorenflo and Kenning, 2010).

In this method, a reduced heat transfer coefficient α/α_0 has been established where the influence on α of the main groups of variables, i.e. the properties of the liquids, the nature of the heated surfaces, and the operating parameters (viz. the heat flux q and pressure p) are treated separately. Thus

$$\frac{\alpha}{\alpha_0} = F_q \cdot F_{p^*} \cdot F_{wR} \cdot F_{wM} \tag{4}$$

with α_0 being the heat transfer coefficient for a *specific* fluid at a reference state that is the same for *all* fluids, and F_q, F_{p^*}, F_w are independent non-dimensional functions applicable to *all* fluids (with a very small number of exceptions), representing the *relative* influences on α of the heat flux q, the reduced pressure p^* (caused by the change in fluid properties with p^*) and wall properties (F_{wR} for the surface roughness and F_{wM} for the material of the wall).

The reference conditions are typical mid-range values for fully developed nucleate boiling in industrial applications: $q_0 = 20$ kW/m^2 and $p_0{}^* = 0.1$. The reference state for the heater is defined as a copper cylinder with an intermediate value $R_{a0} = 0.4$ μm of the arithmetic mean roughness height of the surface (as defined in ISO 4287/1:1984) which lies within the range common for heater surfaces manufactured in practice.

The $\alpha(q)$-relationship is expressed by

$$F(q) = \left(\frac{q}{q_0}\right)^n \text{ or } \frac{\alpha}{\alpha_0} = \left(\frac{q}{q_0}\right)^n \text{ and } n = n(p^*) = 0.95 - 0.3p^{*0.3} \tag{5}$$

with the exponent n corresponding to the slopes of the dot-dashed straight lines for constant reduced pressure in the log,log-diagrams of Fig. 5, and the $\alpha(p^*)$-relationship is described by

$$F(p^*) = \frac{\alpha}{\alpha_0} = 0.7p^{*0.2} + 4p^* + \frac{1.4p^*}{1-p^*} \tag{6}$$

at constant heat flux $q_0 = 20$ kW/m^2 (dotted vertical line in Fig. 5) for surface roughness R_{a0} and copper as wall material.

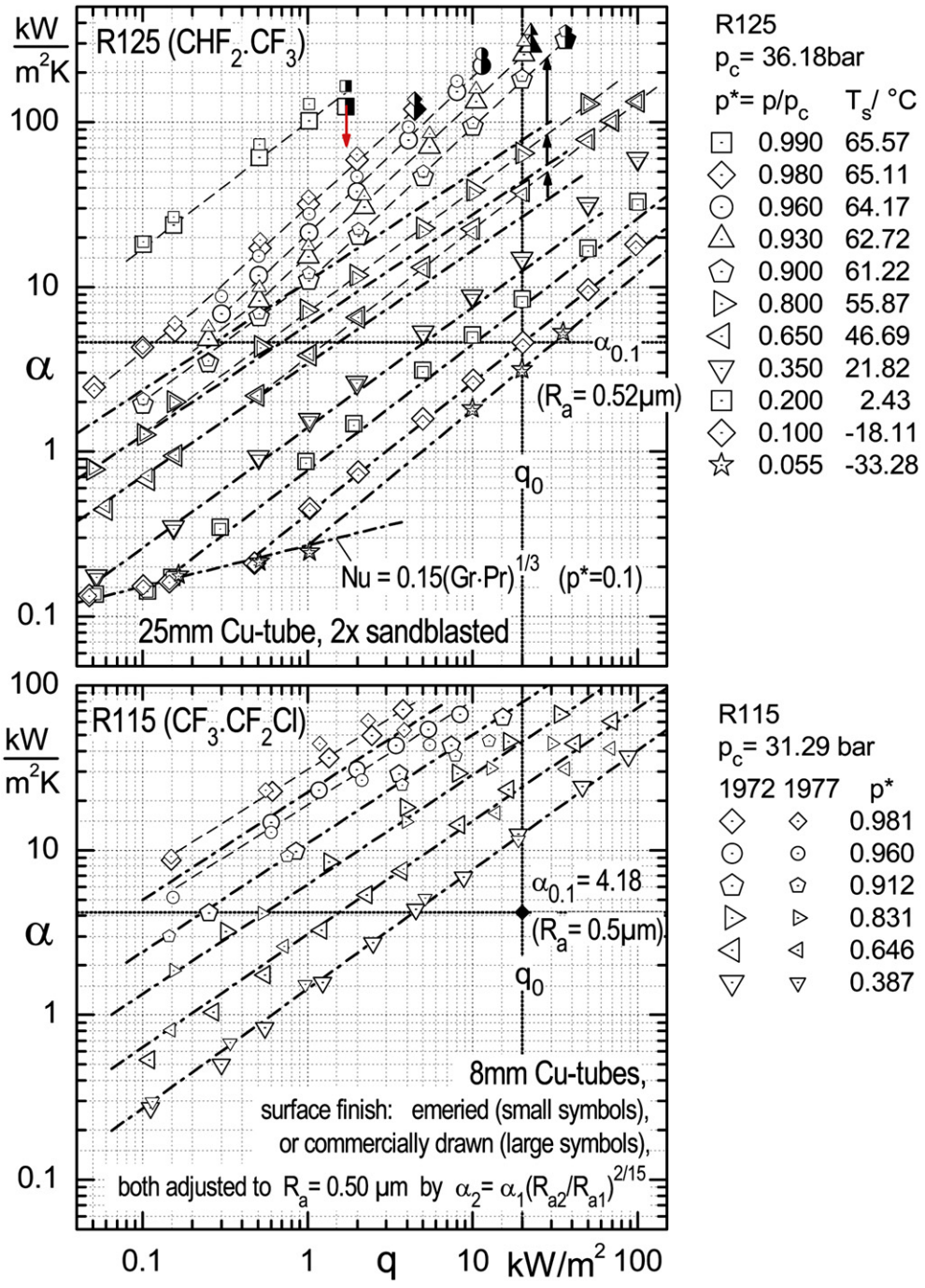

Fig. 5 – Top: Data of Fig. 3, top, compared with updated VDI-Heat Atlas calculation method (dot-dashed lines). Bottom: Former measurements for R115 boiling on 8 mm Cu tubes with emeried or commercially drawn surface and comparison with updated VDI-Heat Atlas calculation method (dot-dashed lines); acc. to Wickenhäuser (1972), Bier et al. (1977a).

(The updated increases of α with q and p^* according to Eqs. (5) and (6) are somewhat more pronounced than in the former calculation method.)

For the influence of the roughness, the relation $\alpha \propto R_a^{2/15}$ is used (as before the update), which was established by Stephan (1963) and which is expressed here in terms of the reference roughness R_{a0}:

$$F_{wR} = \left(\frac{R_a}{R_{a0}}\right)^{\frac{2}{15}}. \quad (7)$$

Originally, a different parameter in the former German standard DIN 4762/1:1960 was chosen by Stephan because it could be related to the volume of vapour trapped in the roughness cavities of the heating surface. This relationship is not implied, however, by any of the parameters defined in the new standard ISO 4287/1:1984, but it was shown by Schömann (1994) and in former editions of the VDI-Heat Atlas that a power law relationship exists between the former parameter and R_a that is valid over a large range of R_a-values and that the

reference value chosen here, $R_{a,0} = 0.4\ \mu m$, is a representative value for metal surfaces.

Furthermore, $F_{wM} = 1$ because the wall material for the data in Figs. 3–5 is the same as the reference material (copper). The reference heat transfer coefficient α_0 for a *specific* fluid is calculated by

$$\alpha_{0,calc} = 3.58\,P_f^{0.6},\ \text{with} \qquad P_f = \frac{\left(\frac{dp}{dT}\right)_{sat}}{\sigma} \tag{8}$$

where $(dp/dT)_{sat}$ is the slope of the vapour pressure curve and σ is the surface tension, both at the reference pressure $p_0^* = 0.1$.

The reference heat transfer coefficients calculated from Eq. (8) for the two fluids of Fig. 5 are

$$\alpha_{0,calc} = 4.43 kW/m^2K \quad \text{for} \quad R125 \quad \text{and}$$
$$\alpha_{0,calc} = 4.06 kW/m^2K \quad \text{for} \quad R115.$$

For the experimental surface roughness $R_{a,exp} = 0.52\ \mu m$ within the area containing the main cross section on the 25 mm tube,

$$\alpha_{0.1} = \alpha_0 \cdot \left(R_{a,exp}/R_{a0}\right)^{2/15} = 4.59 kW/m^2K$$

is calculated from Eq. (7). It coincides with the experimental value for q_0 and $p_0^* = 0.1$ in the upper diagram of Fig. 5 (large rhomb). In case of the 8 mm tubes, the experimental roughness was 0.16 μm for the drawn and 0.36 μm for the emeried surface. For the comparison with R125, the experimental data for R115 with the two surface treatments denoted by large or small symbols in the lower diagram were adjusted to $R_a = 0.5\ \mu m$ using Eq. (7), and the reference value follows from Eq. (7):

$$\alpha_{0.1} = \alpha_0 \cdot (0.5/0.4)^{2/15} = 4.18 kW/m^2K.$$

(The reference values for R125 and R115 are called $\alpha_{0.1}$ instead of α_0 because one of the reference conditions is not fulfilled: $R_a = 0.52$ or 0.5 μm instead of 0.4 μm.)

As can be seen from the lower diagram of Fig. 5, the agreement between experimental and calculated results is very good up to $p^* = 0.91$, particularly for the commercially drawn surface (large symbols), and even for $p^* = 0.96$, the deviations are comparatively small, despite the fact that the range of validity for Eq. (6) ends at $p^* = 0.9$. The deviations of the experimental data for the emeried surface to lower α-values at high heat fluxes for almost all pressures investigated indicate that additional heat transfer resistances might have existed within the tube, due to somewhat less homogeneous soft soldered connections than in the case of the drawn tube.

For R125 and the twice sandblasted tube, the calculated α-values also agree very well with the experiments for the four lower reduced pressures (upper diagram of Fig. 5). From $p^* \geq 0.65$ upwards, however, this holds only for low heat fluxes, while the experimental data at high heat fluxes deviate increasingly from the calculated results (see the vertical arrows). Again the many, similar, small cavities produced during the 1st blasting run and the tiny bubbles at

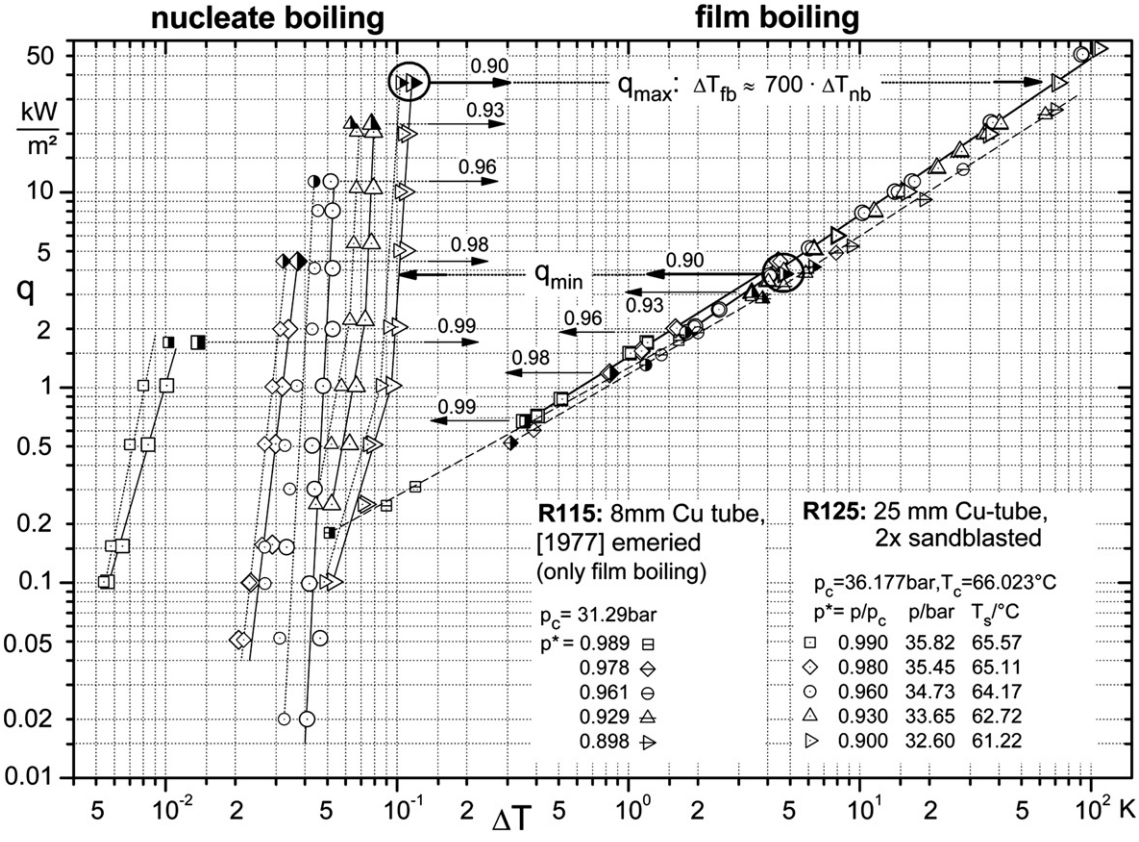

Fig. 6 – Transition between nucleate and film boiling. Earlier data of R115/8 mm (acc. to Bier et al., 1977b) at $p^* \geq 0.9$ and comparison with new results for R125/25 mm.

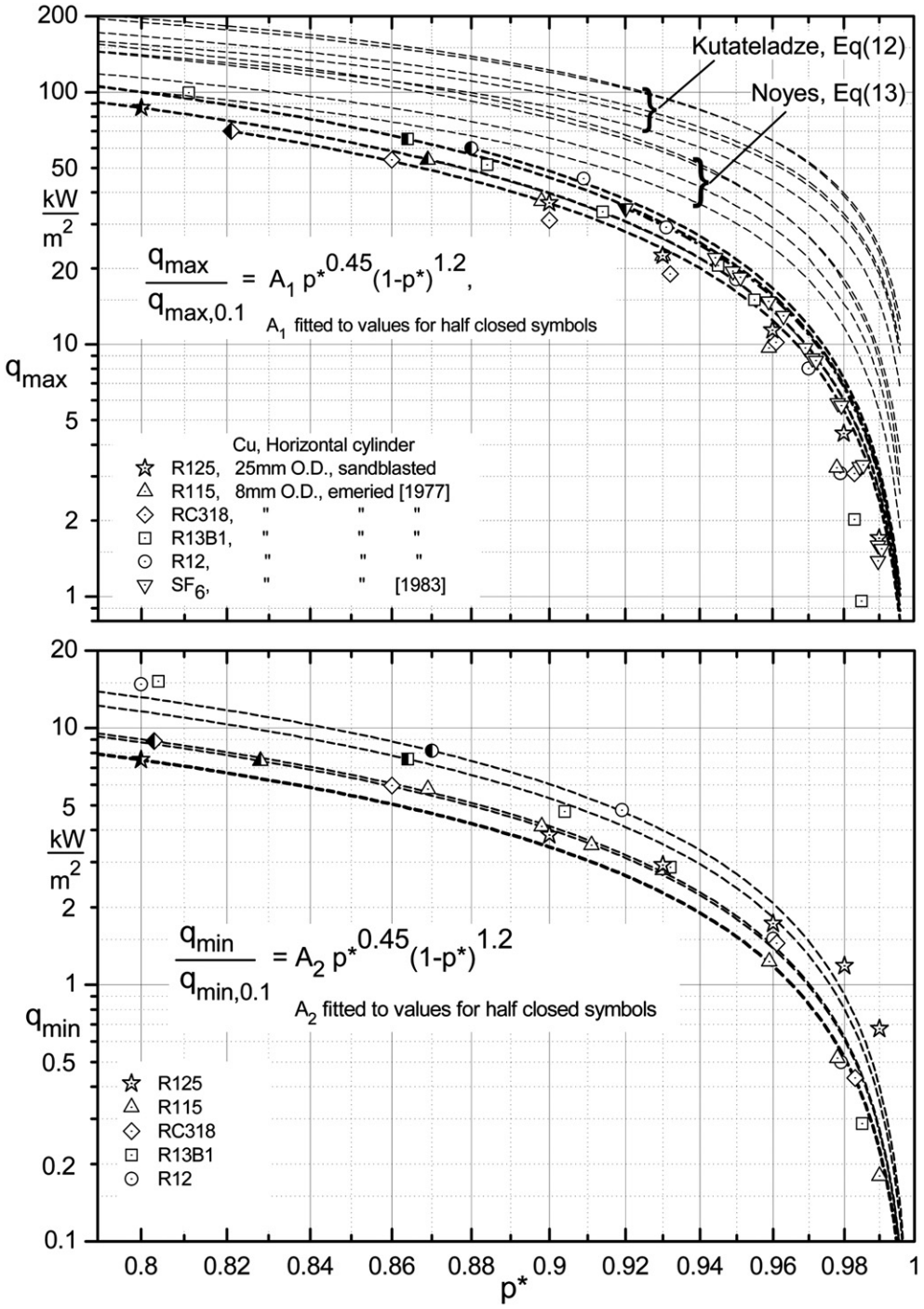

Fig. 7 – Pressure dependence of q_{max} (top) and q_{min} (bottom) at high reduced pressures $p^* \geq 0.8$ and comparison with Eq. (9) fitted to half-filled data points; for q_{max} (top), also with Eqs. (12) and (13) of Kutateladze and Noyes.

high p^* may have been the reason, as discussed for Figs. 3 and 4.

The half-closed symbols in the upper diagrams of Figs. 3 and 5 and the arrows pointing to the right (Fig. 3) or downward (Fig. 5) indicate the well-known fact that nucleate boiling ends at a certain maximum heat flux and **film boiling** occurs *at the same heat flux* – preset by the electrical power input to the test tube –, but at much higher superheats of the tube.

4. Film boiling

4.1. *Transition between nucleate and film boiling*

As can be seen from the five high reduced pressures in Fig. 6, nucleate boiling ends for $p^* = 0.90$ at $q_{max} = 36\ kW/m^2$ because neighbouring bubbles growing on the tube surface are combining to a vapour blanket around the tube and **film**

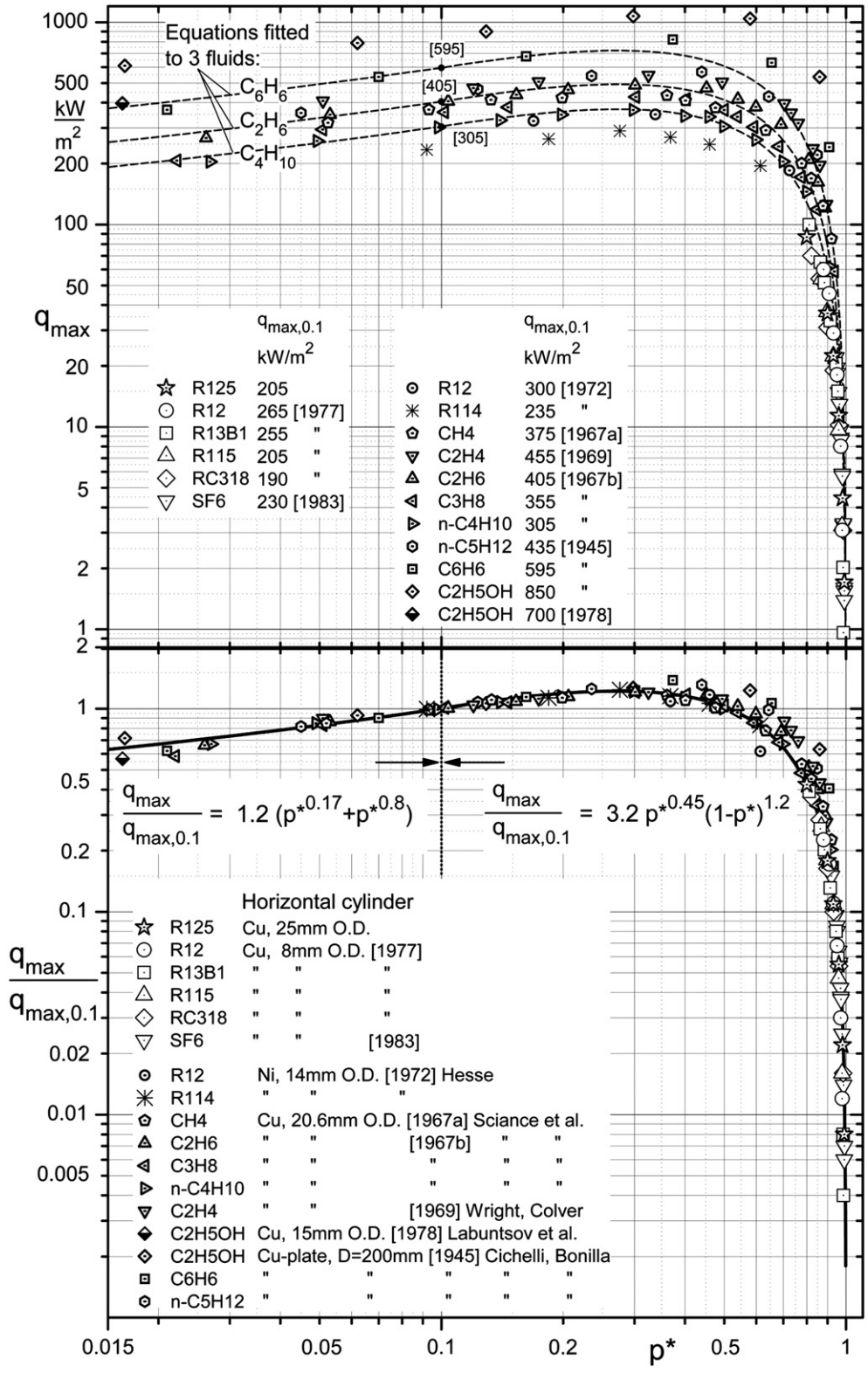

Fig. 8 – Pressure dependence (top) and relative pressure dependence (bottom) of q_{max} and comparison with data from literature and with Eqs. (9) and (11).

boiling starts. Now much higher ΔT-values are necessary for transfer of the same heat flux than at nucleate boiling, due to the insulating effect of the vapour layer (see the highest arrows pointing to the right and the triangle at $\Delta T = 72$ K).

With film boiling established, q was decreased in the experimental runs for constant pressures (see Fig. 6, on the right), and there another well-known effect happens, because at a certain minimum heat flux q_{min} (or superheat ΔT_{min}), the

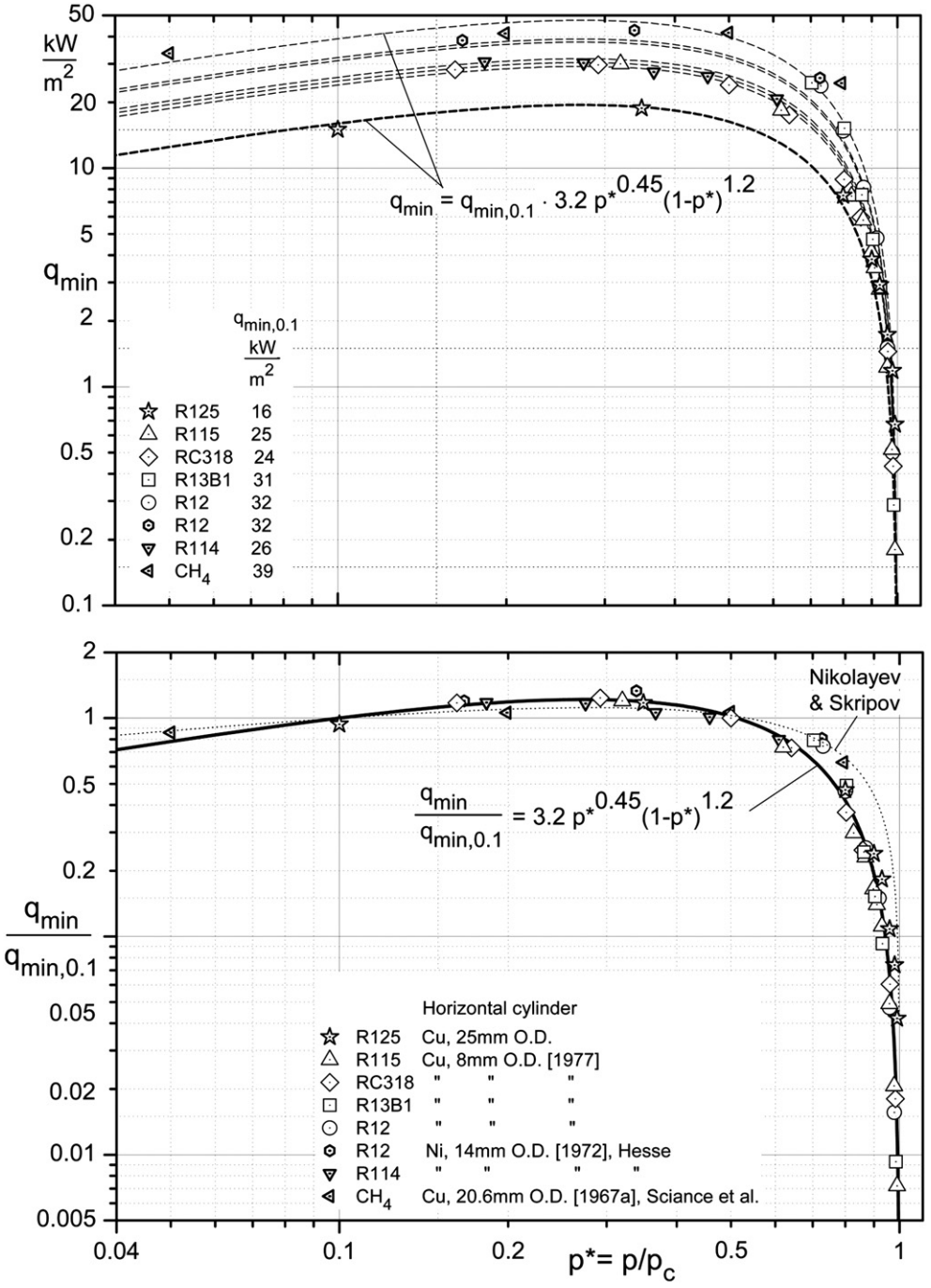

Fig. 9 – Pressure dependence (top) and relative pressure dependence (bottom) of q_{min} and comparison with data from literature and with Eqs. (9) and (14).

vapour blanket around the tube collapses (see e.g. the half-filled triangle at $\Delta T = 4.7$ K and the arrows for $p^* = 0.90$ pointing to the left), and nucleate boiling appears again, with much smaller ΔT than at film boiling.

Unlike nucleate boiling, heat transfer coefficients in film boiling are significantly less dependent on pressure. The end of nucleate boiling, q_{max}, and the end of film boiling, q_{min}, however, decrease markedly with increasing reduced pressure (within this range of very high p^*), see the arrows for rising p^* in Fig. 6 and the results shown in Figs. 7–9.

Earlier measurements (Bier et al., 1977b) for film boiling of the subsequently outdated refrigerant R115 ($CF_3.CF_2Cl$) on an emeried Cu tube with 8 mm O.D. (see symbols with dash) have been added in Fig. 6 for the five reduced pressures investigated with both tubes. The comparison reveals that the film boiling data for both fluid–tube combinations agree well, except that q_{min} for R125 on the 25 mm tube becomes increasingly higher than for R115 on the 8 mm tube as p^* increases beyond $p^* = 0.96$ (cf. half-closed circles, rhombs, squares without or with dash).

In the following figures, a detailed comparison of q_{max} and q_{min} is given for the new experimental results of R125 boiling on the 25 mm Cu tube, with earlier measurements for other fluids and heating elements, and also with correlations.

The comparison focusses on the pressure range $p^* \geq 0.8$, which contains by far the greatest variation of q_{max} and q_{min}. The new measurements of q_{max} for R125 were restricted to this range so that q should not exceed $q = 100$ kW/m^2 for safety reasons.

The same restriction holds for earlier tests of other refrigerants (and SF_6) boiling on the emeried 8 mm tube already mentioned in Figs. 5 and 6 (symbols in the upper diagram; Bier et al., 1977b). The tests with SF_6 were focussed on q_{max} for mixtures at high reduced pressures (Alpay and Gorenflo, 1983) and were not extended to film boiling. Therefore no q_{min}-data are given for this fluid.

These data are plotted at high resolution in Fig. 7, q_{max} in the upper diagram, q_{min} in the lower diagram, together with various correlation lines for their relative pressure dependence based on previous studies at lower values of p^*. The same data (large symbols) are shown together with experimental data from the literature for some further fluids (small bold symbols) over a wide range of p^* in Fig. 8 (q_{max}) and Fig. 9 (q_{min}). The values of q are plotted in the upper diagram of each Figure and their *relative* pressure dependence is shown in the lower diagrams.

The correlation used in Figs. 8 and 9 to predict the *relative pressure dependence* of q_{max} and q_{min},

$$q = q_{0.1} \cdot 3.2 p^{*0.45} (1 - p^*)^{1.2}, \tag{9}$$

is a modification of the function for q_{max} in the VDI-Heat Atlas,

$$q_{max} = q_{max,0.1} \cdot 2.8 p^{*0.4} (1 - p^*), \tag{10}$$

that was established by Gorenflo (1982) based on studies of Borishanskij (1969) and Mostinskij (1963). For $p^* \geq 0.8$, however, the pressure dependence of Eq. (10) is significantly too weak for q_{max} as was shown in Gorenflo et al. (2009).

For pressures below $p^* = 0.1$, the $q_{max}(p^*)$-relationship is correlated by

$$q_{max} = q_{max,0.1} \cdot 1.2 \left(p^{*0.17} + p^{*0.8}\right) \tag{11}$$

because it is distinctly less pronounced than Eq. (9) would predict, as follows from measurements of Labuntsov et al. (1978) for ethanol and water ranging down to $p^* \approx 10^{-4}$. (The half-closed rhomb in both diagrams of Fig. 8 corresponds to the highest p^* investigated in the pertaining tests.) The relationship is similar to that for liquid metals, which can be described by $q_{max} \sim p^{*m}$ where $0.15 < m < 0.20$ – a condition that is met by the first term of Eq. (11), being dominant within the range of very low p^*.

Eqs. (9) and (11) predict the *relative pressure dependence* of q_{max} from the experiments quite well, with the exception of the pioneering data of Cichelli and Bonilla (1945) for a Cu-plate with $D = 200$ mm, that remain comparatively high at pressures $p^* > 0.4$, beyond the maximum of the curve – as can be seen more clearly from the absolute values in the upper diagram of Fig. 8.

The reference values $q_{max,0.1}$ derived from the experiments (and listed in Fig. 8, top) are compared in Table 1 with data calculated from two selected correlations developed by Kutateladze (1952; cf. also: Zuber, 1958; Zuber et al., 1961)

$$q_{max} = A_3 \Delta h_{sat} \rho_v^{0.5} [\sigma(\rho_l - \rho_v) g]^{0.25} \equiv A_3 \cdot \text{'Ku'}, \tag{12}$$

with $A_3 = 0.13 \ldots 0.16$, and Noyes (1963)

$$q_{max} = A_4 \cdot \text{'Ku'}, \tag{13}$$

with $A_4 = 0.144\ [(\rho_l - \rho_v)/\rho_l]^{0.25}$, where Δh_{sat} is the enthalpy of vaporization, σ is the surface tension, and ρ_v and ρ_l are the densities of vapour and liquid, respectively. (Zuber derived $A_3 = 0.13$ from a simplified model for the development of instability in the counter-flow of liquid and vapour normal to a horizontal plate. A review of more correlations containing the term 'Ku' is given in Alpay and Gorenflo, 1983.)

The comparison in Table 1 shows that $q_{max,0.1}$ calculated from Eq. (12) lies above the experimental values in most cases, while for Eq. (13), it is mainly vice versa, but with smaller differences. Similar deviations result from recent measurements of Kang et al. (2009) for five refrigerants at $T_{sat} = 7$ °C (corresponding to $0.012 < p^* < 0.17$). Their experimental runs at $p = \text{const}$ for electrically heated 8 mm Cu tube also end at q_{max} without any deviation from the $\alpha(q)$-behaviour at lower heat fluxes, in the same way as is shown in Fig. 6.

From the expanded scale in the upper diagram of Fig. 7, it can be seen that the relative pressure dependence of *both correlations*, Eqs. (12) and (13), is significantly too weak at $p^* > 0.8$ for the fluids included in that diagram. The same also follows from results in (Haramura, 1999) for ethanol, water, nitrogen and helium (at $p^* > 0.9$ data are given only for the last fluid).

Therefore, Eq. (9) is more appropriate for prediction in this pressure range, preferably fitted to q_{max} from experiments at a high value of p^* by changing A_1, or if unavailable, to $q_{max,0.1}$ from Eq. (13) – the latter resulting either in q_{max}-values "on the safe side", or compensation for the opposite deviations (of Eq. (13) at $q_{max,0.1}$ and Eq. (9) at very high p^*), in trend at least.

Table 1 – . Experimental reference values $q_{max,0.1}$ at $p^* = 0.1$ for the fluids shown in Fig. 8 and comparison with Eqs. (12) and (13).

Fluid		$q_{max,0.1}$ (kW/m^2)		
		exp.	Eq. (12)	Eq. (13)
CH_4	1967a	375	385	365
C_2H_4	1969	455	455	423
C_2H_6	1967b	405	451	411
C_3H_8	1967b	355	409	344
n-C_4H_{10}	1967b	305	374	301
n-C_5H_{12}	1945	435	347	271
C_6H_6	1945	595	496	396
C_2H_5OH	1945	850	870	626
C_2H_5 OH	1978	700[a]	870	626
SF_6	1983	230[b]	273	214
R12	1972	300[b]	322	271
R12	1977	265[b]	322	271
R13B1	1977	255[b]	285	239
R114	1972	235	261	202
R115	1977	205[b]	242	185
R125	2009	205[b]	304	237
RC318	1977	190[b]	230	160

a Extrapolated from lower p^*.
b Extrapolated from higher p^*.

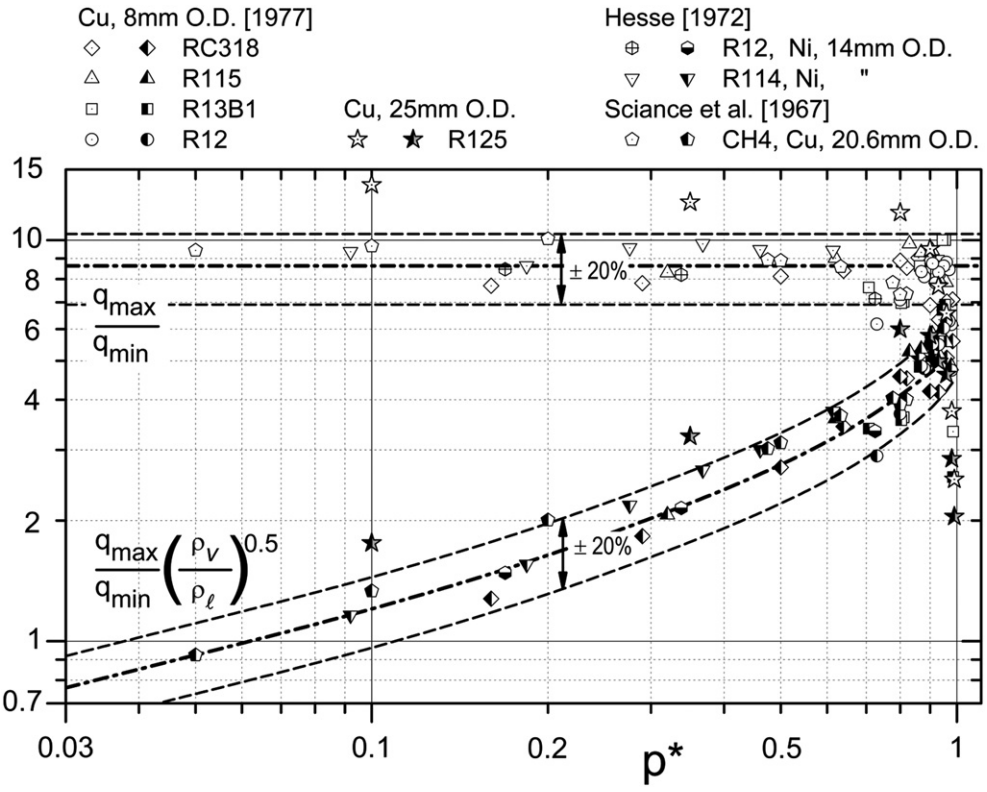

Fig. 10 – Pressure dependence of the ratio q_{max}/q_{min} (open symbols) and after modification with the density ratio of vapour and liquid (half-filled symbols).

The comparison of the experimental data for q_{min} with Eq. (9) in Fig. 9 demonstrates that the *relative pressure dependence* following from the measurements is well correlated by Eq. (9) for all fluids – apart from a few data points at $p^* = 0.7$ and 0.8. As to the *absolute values*, the earlier results for the 8 mm tube agree well with the data of Hesse (1972) for R12 and R114 and a 14 mm tube (cf. R12 near $p^* = 0.7$ and R114/R115 between $p^* = 0.3$ and 0.6).

However, the new q_{min}-values for R125 and the 25 mm tube, as already discussed above, are much smaller at $p^* = 0.1$ and 0.35 than expected for this fluid from the earlier data for the other fluids (and the 8 mm tube), – and vice versa at the two highest p^* (better seen in Fig. 7).

In the lower diagram of Fig. 9, a correlation developed by Nikolayev and Skripov (1970), which is recommended by Nishio (1999) has also been added (dotted curve),

$$q_{min} = q_{min,0.1} \cdot A_5 \cdot p^{*0.24}(1 - p^*)^{0.61} \quad (14)$$

with $A_5 = 1.853$ modified for the reference pressure $p^* = 0.1$ used here (in the original version, it was normalized to $p^* \approx 0.34$ with $A_6 = 1.67$ or $p^* = 0.9$ with $A_7 = 4.18$, respectively). Eq. (14) was derived from experiments of the authors with three tubes (approx. 4 mm O.D.) and various fluids, but with wide scatter of the data points, even for the same pressure and fluid.

As can be seen, the deviations between the two correlations, Eqs. (9) and (14), remain within the experimental scatter for $0.05 \leq p^* \leq 0.7$ (with the maximum of Eq. (14) at $p^* \approx 0.28$ and of Eq. (9) at $p^* \approx 0.27$). Approximately the same holds for a correlation proposed by Kutateladze (1963), while substantial deviations occur for two others (Zuber, 1958; Lienhard and Wong, 1964).

For $p^* > 0.8$, however, the relative pressure dependence of q_{min} from Eq. (14) is too weak amounting only to about half the decrease of R125 and the 25 mm tube, which is the least found in the experiments shown in Figs. 7 and 9.

In Fig. 10, the ratio q_{max}/q_{min} (open symbols) for the new measurements with R125 and the 25 mm tube and the product of this ratio with the square root of the density ratio of vapour and liquid (half-filled symbols) is compared with the former data for the four other refrigerants and the 8 mm tube, and with some other data from literature.

According to the correlations of Zuber for q_{max} and q_{min}, the product of the ratios should be constant at 0.76, independent of the pressure and the nature of the fluid (Zuber, 1968). While the experimental scatter for the various fluids remains within approx. ±20% (half-filled symbols), there is a clear pressure dependence with markedly higher values of the product – that arrive, however, near 0.76 for $p^* \approx 0.03$ (cf. the left lower corner of the diagram) which approximately corresponds to $1 < p < 2$ bar for most organic fluids.

Instead, the ratio of the heat fluxes even *without the density ratio* seems to be independent of p^* and the fluid within ±20%, apart from a few exceptions. For the new results of R125, however, the ratio deviates to higher or lower values, respectively, at the three lowest or highest pressures investigated. This is consistent with the systematic deviations of q_{min} for the 25 mm tube as discussed in connection with Figs. 7 and

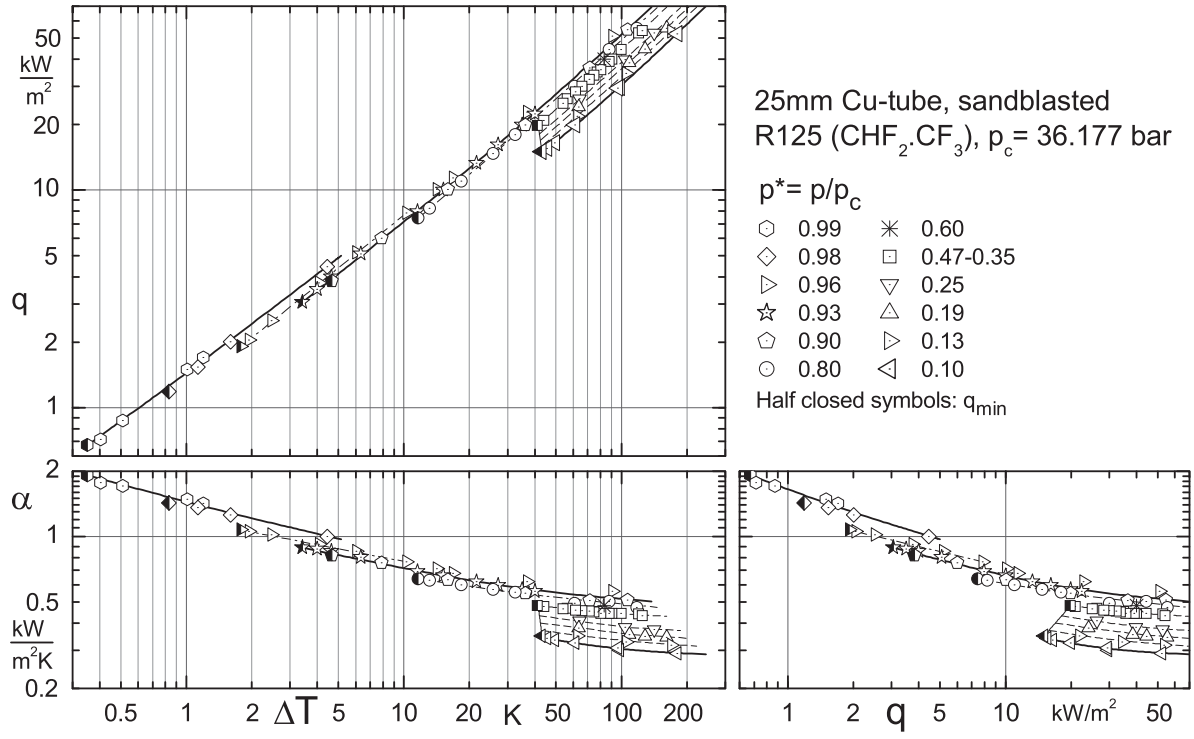

Fig. 11 – Film boiling of R125 on a horizontal 25 mm Cu tube: all new experimental results in three log,log-representations.

9. (It should be noted that for $p^* < 0.8$, only the data points from Hesse (1972, 1973) and Sciance et al. (1967a,b) are based on experimental results for *both*, q_{max} and q_{min}; for the rest, Eq. (9) has been used to extrapolate q_{max} from $p^* \geq 0.8$.)

4.2. *Film boiling heat transfer*

In Fig. 11, the new measurements of film boiling heat transfer for R125 at $p^* < 0.9$ have been added to those of Fig. 6 near CP, and the $q(\Delta T)$-representation has been completed by $\alpha(\Delta T)$- and $\alpha(q)$-plots. Unlike nucleate boiling, α *decreases* with increasing q and ΔT, respectively, in the range of superheats ΔT investigated here, which are small compared to film boiling applications in practice, so heat transfer by radiation from the heated wall to the liquid through the vapour film can be neglected.

The influence of pressure on α is somewhat more pronounced than in single-phase free convection at low p^* but much less than in nucleate boiling (cf. e.g. the corresponding

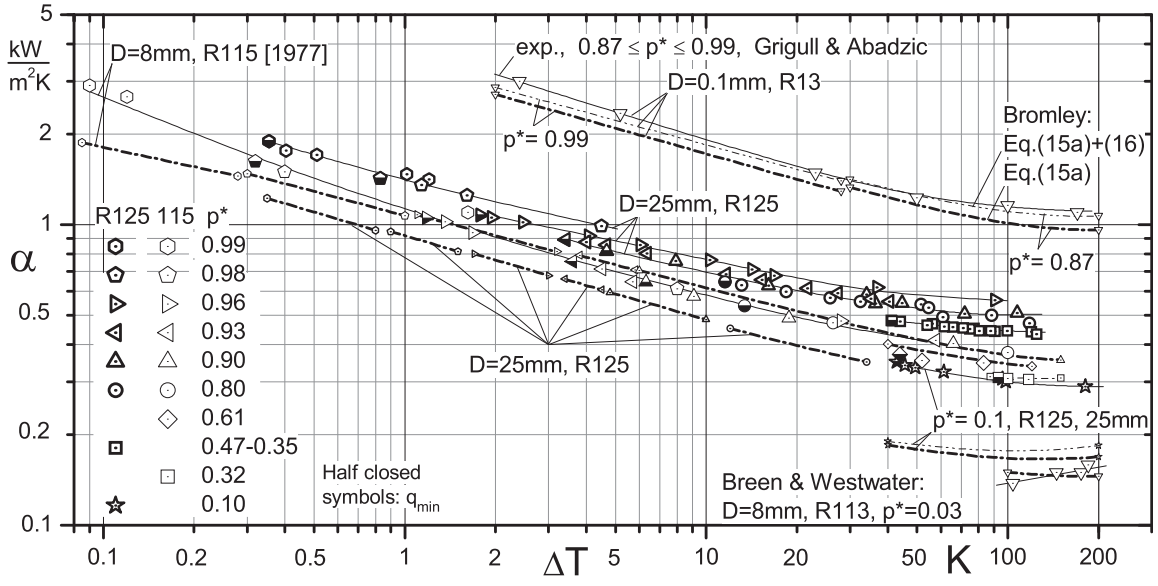

Fig. 12 – New results of Fig. 11 compared with former experimental data for R115/8 mm, R113/8 mm, R13/0.1 mm and comparison with Eqs. (15) and (16) developed by Bromley.

lines for both at $p^* = 0.2$ and 0.025 in Fig. 3, bottom). Very close to CP, the influence increases, even for small variations of p^* (cf. $p^* = 0.96$ and 0.98 in the $\alpha(q)$-plot which is most sensitive for this effect), due to the greater variation of thermophysical properties in this region.

Here, the governing variable is $[1 - p^*]$ or the distance from CP, while at lower pressures, it is p^*, with a clearly systematic decrease of α with p^* that levels out near the highest heat fluxes investigated – for all reduced pressures (the slightly deviating behaviour of the run for the squares is caused by the variation of p^* during this run – highest ΔT or q belonging to $p^* = 0.47$ and lowest to 0.35 – because the data were taken while trying to measure q_{min} at the lowest p^* possible).

The new results for R125 and the 25 mm tube at $p^* \geq 0.9$ and the three systematic runs at lower p^* (0.8; ~0.4; 0.1) are compared in Fig. 12 with measurements for other fluids and heaters and with a calculation method of Bromley in its simplified form (Bromley, 1950)

$$\alpha = 0.62(D\Delta T)^{-0.25}\left(\frac{g\lambda_v^3\rho_v\Delta h\Delta\rho}{\eta_v}\right)^{0.25} \tag{15}$$

where λ_v, ρ_v, η_v are the thermal conductivity, density and dynamic viscosity of the vapour, evaluated at $T_m = 0.5(T_w + T_l)$, and $\Delta\rho = \rho_l(T_{sat}) - \rho_v(T_m)$, $\Delta h = h_v(T_m) - h_l(T_{sat})$ are the differences in density and specific enthalpy between the vapour and the liquid. $\Delta T = T_w - T_l$ (with $T_l = T_{sat}$) is the superheat of the wall (as holds throughout the paper).

Eq. (15) can also be expressed in dimensionless form

$$\frac{\alpha D}{\lambda_v} = 0.62\left(\frac{D^3 g\rho_v\Delta h\Delta\rho}{\eta_v\lambda_v\Delta T}\right)^{0.25} \tag{15a}$$

that corresponds to $Nu_D = 0.62(Gr_D \cdot Pr_D)^{0.25}$ for single-phase free convection (or to Eq. (2b) with 0.62 instead of 0.60) if Gr and Pr are defined as in Section 5 with Δh, $\Delta\rho$ (and ΔT) to be taken across the *entire* boundary layer, from the fluid at saturation conditions to the heated wall, differing from Bromley's proposal for Eq. (15) with respect to the reference

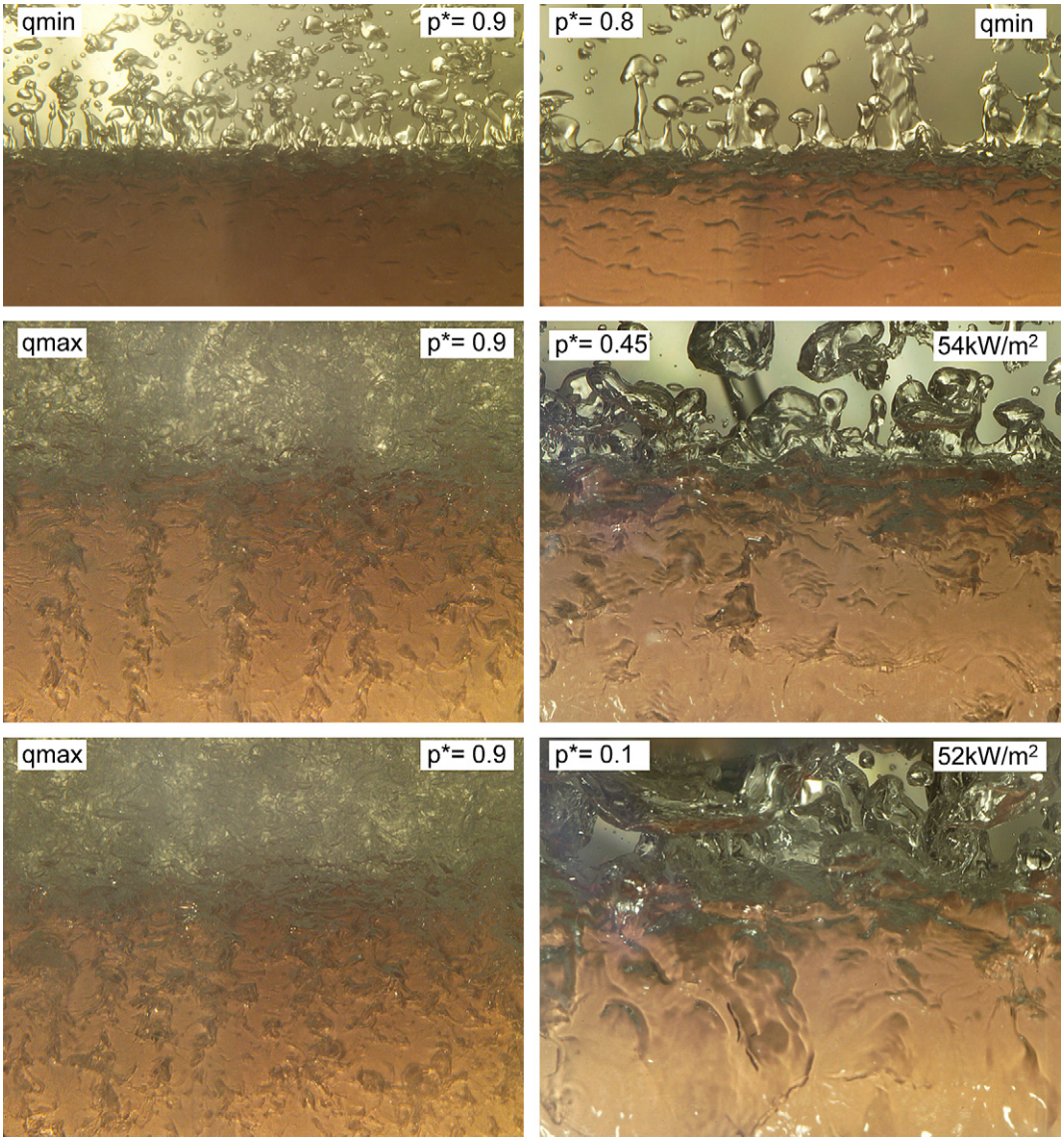

Fig. 13 – Structure of the vapour/liquid interface on the upper parts of the tube and pattern of vapour release from the tube for film boiling of R125 on the 25 mm Cu-tube.

temperature for the vapour, but only in Δh and $\Delta\rho$. (For all calculated data shown in Fig. 12 this modification was used).

The comparison in Fig. 12 between the experimental data (symbols) and the results calculated from Eq. (15a) (bold dot-dashed lines) reveals that the deviations for the 8 mm tubes and the 0.1 mm wire remain within approximately ±10%, except for R115 at $p^* = 0.99$. *The slope* of the calculated curves follows the experimental trend – also at the highest superheats where it deviates from the constant value of −1/4 – according to $\alpha \sim (\Delta T)^{-0.25}$ in Eq. (15) – obviously due to the remarkable variation of the thermophysical properties of the vapour with temperature.

This is even better realized by the upper (fine) dot-dashed lines for R13 (shown also for R115 at $p^* = 0.32$ and R125 at $p^* = 0.1$) which were calculated using an extension of Eq. (15) by the factor

$$\left(1 + 0.34 c_{p,v}\frac{\Delta T}{\Delta h}\right)^{0.5} \qquad (16)$$

originating from Bromley, too (according to Nishio, 1999). In 1952, he proposed to modify the factor 0.34 to 0.4 and to use the latent heat of vaporization Δh_{sat} instead of Δh (Bromley, 1952). For the experimental conditions of Fig. 12, α was calculated from Eqs. (15) and (16) with different factors and also using T_m *or* T_w as reference temperature for the vapour in Δh and $\Delta\rho$, and the scatter of the results according to all the different calculation procedures did not significantly exceed ±10%.

According to Son and Dhir (2008), similar good agreement with Bromley's correlation – and therefore also with the experiments discussed above – is achieved by three-dimensional simulation of saturated film boiling and by correlations of Breen and Westwater (1962) and Sakurai et al. (1990), if $0.3 < D/l_0 < 10$, with $D/l_0 = D/(\sigma/g\Delta\rho)^{0.5}$ = dimensionless diameter (Son and Dhir, 2008). This condition is met by the experiments with R13 and R113 in Fig. 12, but not for R115 where D/l_0 increases from 13 (at $p^* = 0.32$) to 76 ($p^* = 0.98$), and yet there is good agreement with Eqs. (15) and (16).

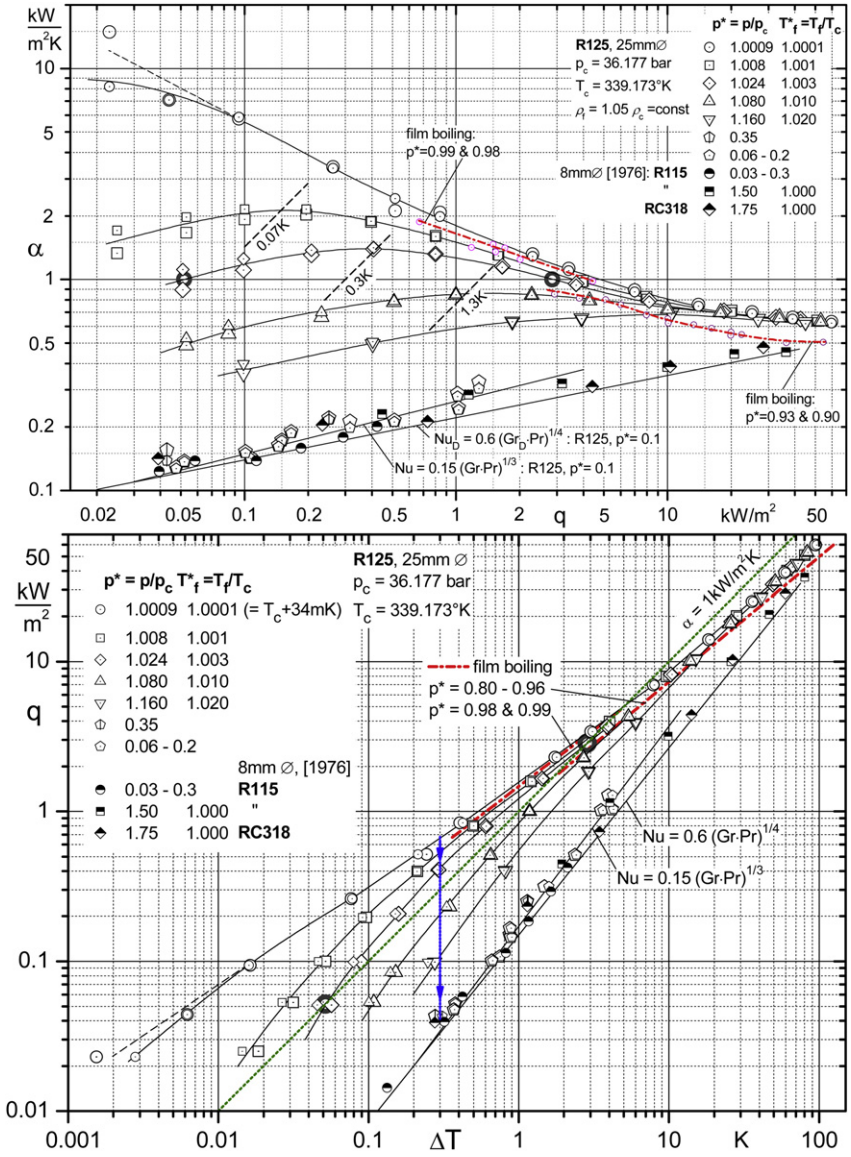

Fig. 14 – Single-phase free convection of R125 on the 25 mm tube near the Critical Point and in greater distance, and comparison with near-critical film boiling (dot-dashed lines).

On the other hand, the deviations between experimental and calculated results for R115 at $p^* = 0.99$ indicate that the influence of the great variation of some properties on film boiling heat transfer is not correctly predicted by Eq. (15) very close to CP, as long as this condition also holds for the vapour, i.e. the superheat ΔT is small. It should be pointed out here that for nucleate boiling, the superheats during the entire experimental runs at $p^* \geq 0.9$ (Fig. 6) were smaller than all the ΔT-values shown for film boiling in Fig. 12 – except for the one with $\Delta T < 0.1$ K. The influence of the property variation close to CP will be discussed more in detail together with the near-critical measurements at $p^* > 1$ in Fig. 20.

In case of the new experimental results for R125 and the 25 mm tube, only the *relative* $\alpha(\Delta T)$-dependence is equally well predicted by Eqs. (15) and (16) at $p^* \leq 0.98$ as for R115 and the 8 mm tube. The *absolute* experimental α-values for the big tube, however, are significantly higher than for the smaller diameter, while the prediction by Eq. (15) is vice versa (lower sequence of dot-dashed lines in Fig. 12) as could be expected from the assumptions in the calculation (smooth vapour–liquid interface and laminar film around a bigger diameter).

The photos in Fig. 13 demonstrate that the assumptions are not valid for this tube because the interface is markedly wavy – at least on the upper parts of the tube that are shown here – and it can be assumed from the way the vapour leaves the tube that turbulent motion exists, with better heat transfer than in the laminar case, cf. also the $Nu(Gr\,Pr)$-representation in Fig. 20 (and the calculations in Sarma et al., 1997 and Hu et al., 2008).

In addition, the irregular pattern of the vapour patches in the four lower photos of Fig. 13 for high heat fluxes indicates that instability criteria with characteristic wavelengths do not dominate in general – perhaps except for very short periods as in the moment of taking the upper photo of the pair on the left taken at the same conditions ($p^* = 0.90$, $q = q_{max} = 36$ kW/m^2).

5. Single-phase free convection

5.1. *Experimental results near the critical state and comparison with film boiling*

In the $\alpha(q)$- & $q(\Delta T)$-diagrams of Fig. 14, the new measurements for single-phase free convection of R125 in the near-critical region are compared with near-critical film boiling data of Fig. 12 for the same heater/fluid-system and with free convection at pressures far below (R115, R125) and significantly above p_c (R115, RC318). For the (bulk) fluid state in the pool that was investigated closest to CP, the temperature T_f was 34 mK (±5 mK) above T_c or $T_f^* = 1.0001$, and the pressure during the run was 33 mbar (±5 mbar) higher than p_c or $p^* = 1.0009$.

The $q(\Delta T)$-plot demonstrates that the new data span the whole range from film boiling (red dot-dashed lines) down to natural convection far from CP ($Nu(Gr \cdot Pr)$-lines). On the one hand, the results for single phase (bulk) fluid states closest to CP ($T^* = 1.0001$ & 1.001) and experimental runs *at constant pressure* are almost the same as at $p^* = 0.99$ & 0.98 for film boiling over the whole ΔT-range investigated there.

At *constant superheat*, however, e.g. $\Delta T = 0.3$ K (vertical line with arrows), q diminishes gradually from $q \approx 0.6$ kW/m^2 very close to CP, down to $q \approx 0.04$ kW/m^2, for free convection both in the far sub-critical range near $p^* = 0.1$ and in the far supercritical range, e.g. $p^* = 1.75$. For the highest superheats investigated, the earlier data for the two supercritical pressures (half-filled rhombs & squares) converge on the new data.

The straight lines for Nusselt numbers – corresponding to Eq. (2) for turbulent or laminar convection (upper or lower line, respectively) – represent the data for both ranges of fluid states quite well (in both diagrams) if the (constant) properties of R125 at $p^* = 0.1$ are used in Nu, Gr, Pr. This is discussed in more detail later in relation to Fig. 20.

The dotted straight line for $\alpha = \text{const} = 1$ kW/m^{2}K in the $q(\Delta T)$-plot reveals by its two intersections with the interpolation curve for the rhombs ($p^* = 1.024$) that maxima are produced in an $\alpha(q)$-representation for runs at $p = \text{const}$, as seen in the upper diagram, a result that had already been found in earlier measurements with three of the four refrigerants cited above and which is shown in Fig. 15 (top) for RC318 (C_4F_8) as an example (from Bier et al., 1976).

The small $p^*(v^*)$-diagram inserted between the two $\alpha(q)$-plots of Fig. 15 shows that the state of the bulk fluid varied along T_c and over a wide range of pressures and densities in those measurements – much wider than in the new runs with $\rho^* = \text{const} = 1.05$ for R125 (see red symbols and vertical line in this diagram).

Another outcome of those tests was that the $\alpha(q)$-maxima only occur if the density ρ_f of the bulk fluid is higher than ρ_c

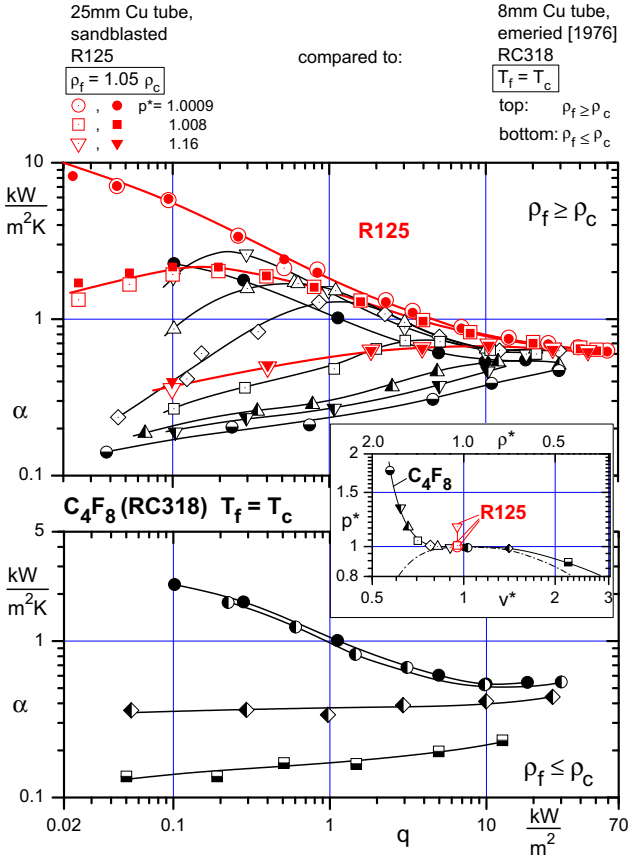

Fig. 15 – Comparison of new near-critical free convection of R125 on the 25 mm tube with RC318 on an 8 mm tube (acc. to Bier et al., 1976).

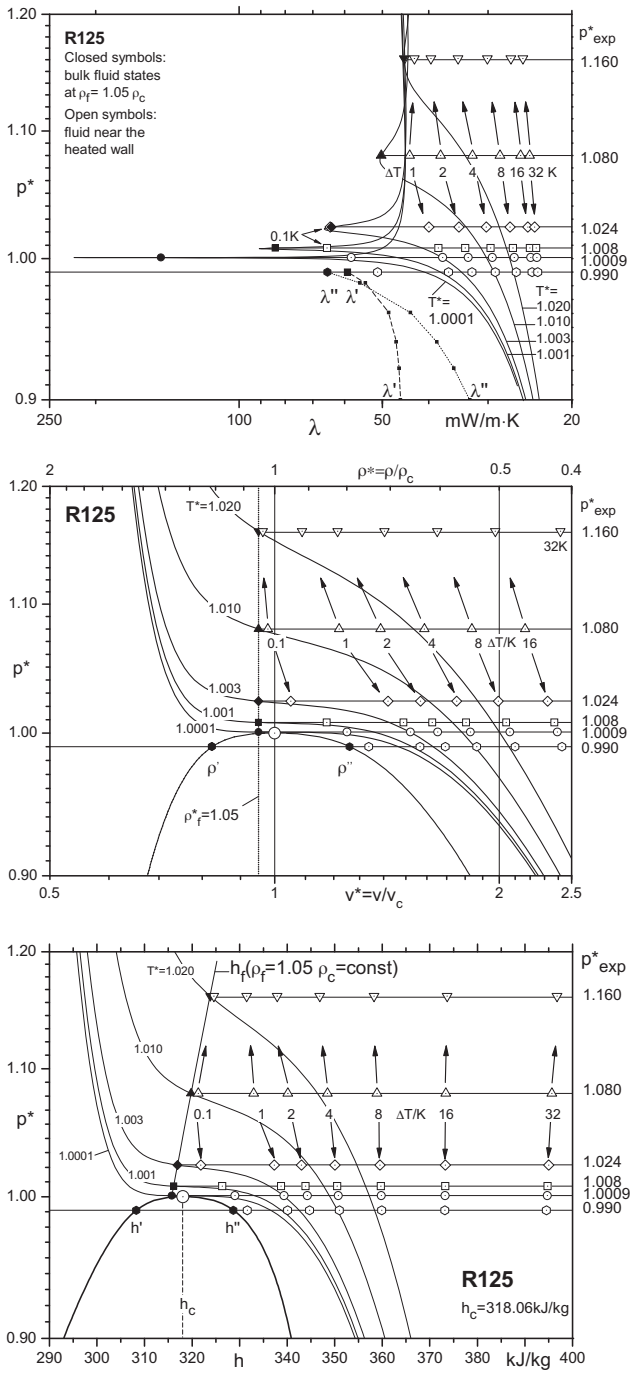

Fig. 16 – Variation of specific enthalpy (bottom), density (middle) and thermal conductivity (top) of R125 near CP and effect of isobaric superheat ΔT.

(for $\rho_f \leq \rho_c$ see the lower diagram of Fig. 15), but not too much, because the maxima are drifting to higher superheats ΔT and vanish, see upper $\alpha(q)$-diagrams of Figs. 14 and 15.

Fig. 15 also demonstrates that the new α-values for the two fluid states closest to CP lie near the triangles representing the earlier data near their maxima, as should be expected from the situation of the (thermodynamic) states of the bulk fluid for R125 or RC318 with respect to CP, shown in the $p^*(v^*)$-diagram. The ΔT-values belonging to three of the new maxima have been included in Fig. 14 (dashed lines, upper diagram) in order to discuss the effect together with the marked variation of some thermophysical properties for isobaric temperature variation near CP.

5.2. *Variation of thermophysical properties*

In the lower diagrams of Fig. 16, specific enthalpy h and density ρ are shown for the five new supercritical runs of Fig. 14 (closed or open symbols = fluid state in the pool or near the heated wall, respectively). The isobaric superheats $\Delta T = 0.1, 1, \ldots 32$ K were arbitrarily chosen and $p^* = 0.99$ was added for comparison with film boiling. As can be seen, density and enthalpy vary drastically between pool and heated wall close to CP, already for the smallest superheat (0.1 K), but the difference decreases rapidly with increasing distance from CP (neighbouring closed and open triangles).

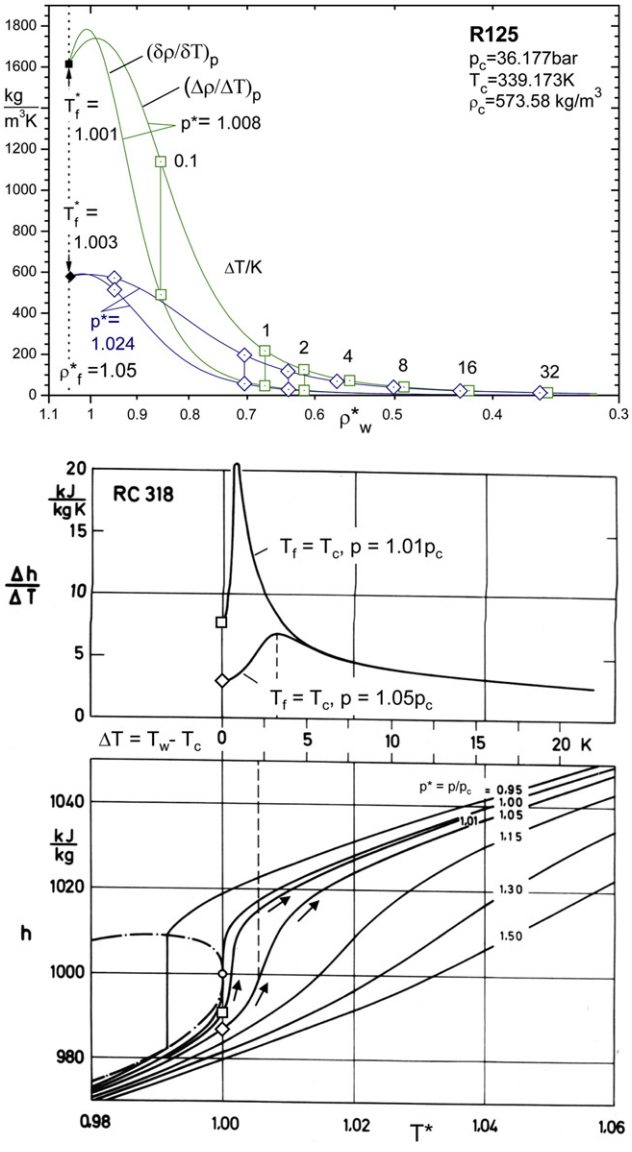

Fig. 17 – Relative variation of density and specific enthalpy near CP and effect of isobaric superheat ΔT. Bottom: RC318 (from Gorenflo, 1977); top: R125.

For film boiling at $p^* = 0.99$, Δh and $\Delta\rho$ between the fluid in the pool (here: saturated liquid) and at the wall for $\Delta T = 0.1$ K are larger than for the two supercritical pressures nearest to CP, but (a) the heat carried away from the wall within the *same volume* of vapour will not differ much because ρ_v is smaller than for $p^* > 1$, and (b) thermal conductivity λ_v is also smaller (upper diagram), so heat transfer to the liquid adjacent to the wall will be diminished. The combined effect of the differences between single-phase and two-phase free convection near CP is more or less exactly compensated, as can be seen from the upper (red) dot-dashed line running between circles and squares in Fig. 14.

While the variation of dynamic viscosity η with temperature and pressure is very similar to h and ρ, the p,T-dependence of the other transport property λ that is included in Gr number, is markedly different. This follows from Fig. 16, top, with an entirely different shape of the isotherms (sharp edges

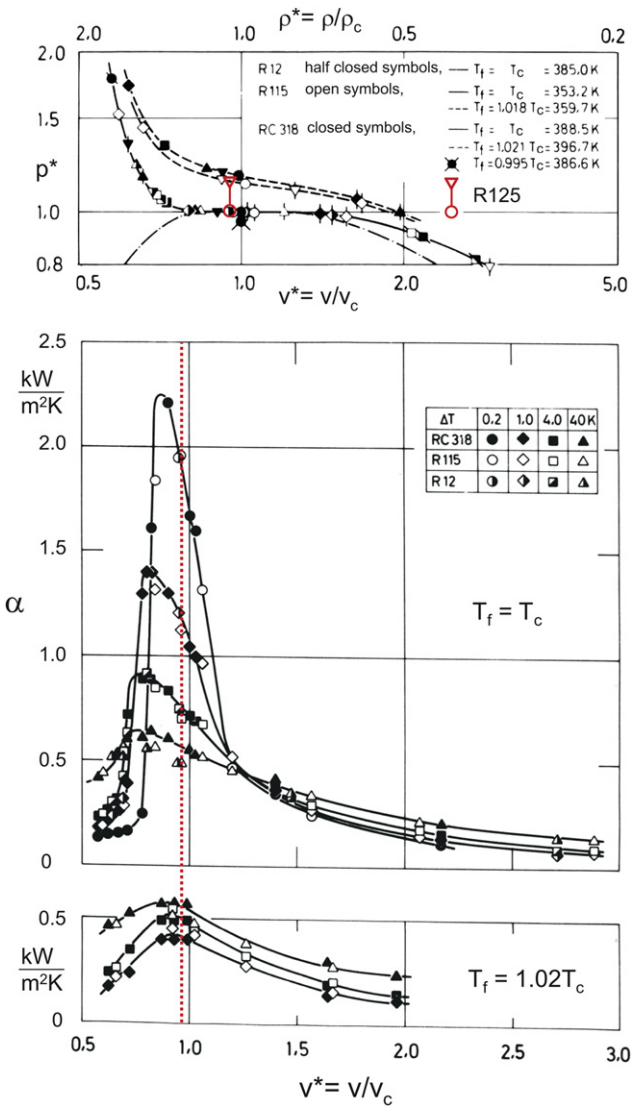

Fig. 18 – Variation of the heat transfer coefficient with reduced specific volume v^* for RC318/8 mm at two temperatures T_f of the pool and various superheats of the tube wall (from Bier et al., 1976, mod.). For comparison: Range of variation for the new measurements with R125/25 mm.

at λ_{max} for the three temperatures closest to T_c) and with vanishing difference between λ for saturated liquid and vapour, already at $p^* < 0.99$ – for the condition of the new measurements, $\rho_f = 1.05\rho_c$ that holds for this diagram, too (because it is the overall condition valid for all new supercritical measurements with R125).

And also the big effect produced by $\Delta T = 0.1$ K near CP decreases much faster than for h and ρ (open and closed symbols for $p^* = 1.024$ coinciding almost entirely), while it remains comparable with the differences between $\Delta T = 1$ & 2 K or 2 & 4 K, respectively, for the two equilibrium properties at this pressure (cf. the lower two diagrams).

Fig. 17 (top and middle) demonstrates in explicit form the large variation of density and enthalpy caused by the isobaric superheat ΔT of the wall for fluid states near CP. In the upper diagram, the maxima of $(\delta\rho/\delta T)_p$ and of the integrated density variation over the entire superheated boundary layer near the wall $(=\Delta\rho/\Delta T)_p$ are shown, that occur already at very small superheats $\Delta T < 0.1$ K, if T_f is close to T_c (for the condition $\rho_f = 1.05\rho_c$ which is preset). And indeed, the same holds for the maximum of α at the same state of the fluid (squares in the upper diagram of Fig. 14 and $\Delta T = 0.07$ K for $T_f^* = 1.001$, $p^* = 1.008$).

In the lower two diagrams of Fig. 17, the same is shown for specific enthalpy h (from Gorenflo, 1977). Here, the shift of $(\Delta h/\Delta T)_p$ to higher superheats ΔT – and the analogy to the shift of the α-maxima – is seen more distinctly, if the distance between CP and state of the bulk fluid increases, because the effect is plotted over T^* (or ΔT), rather than ρ^* as above: ΔT for the maximum increases from $\Delta T = 0.7$ K to ca. 3 K, if the distance increases from $p^* = 1.01$ to 1.05 (with higher absolute ΔT-values for similar p^*, because the data belong to the former refrigerant RC318 or C_4F_8 and the different preset condition $T_f^* = 1$).

α-maxima of entirely different kind occur in Fig. 18, with T_f varying between T_c and 1.02 T_c as in the new measurements, but also ρ_f is varied over a wide range on both sides of ρ_c (acc. to Bier et al., 1976). The α-maxima belong to fluid states with $\rho_f > \rho_c$ ($v_f < v_c$) as in Figs. 14 and 15, but have been produced using *different experimental runs* at p = const and taking α-values for two isotherms T_f and various constant superheats ΔT. For instance, data of RC318 shown also in Fig. 15 appear as closed symbols in the diagram in the middle.

The fluid states of the new measurements with R125 lie between the three isotherms in the upper diagram and slightly on the left of $v^* = 1$ (cf. also Fig. 15), and the data to be extracted from Fig. 14 would appear on a vertical line at $v^* = 0.95$ in the two lower (with data systematically moved to somewhat higher α-values, compared to RC318, as can be concluded from Fig. 15).

The data in the two α-diagrams reveal two separate effects of the marked variation of properties on near-critical free convection:

A. Heat transfer is improved near CP and the *relative* improvement increases with decreasing superheat of the wall in both diagrams, but particularly for fluid states very close to CP (α-maxima in the intermediate diagram), because for small ΔT, also the state of the fluid *near the heated wall* is close to CP (cf. also the comparison with nucleate boiling near CP above).

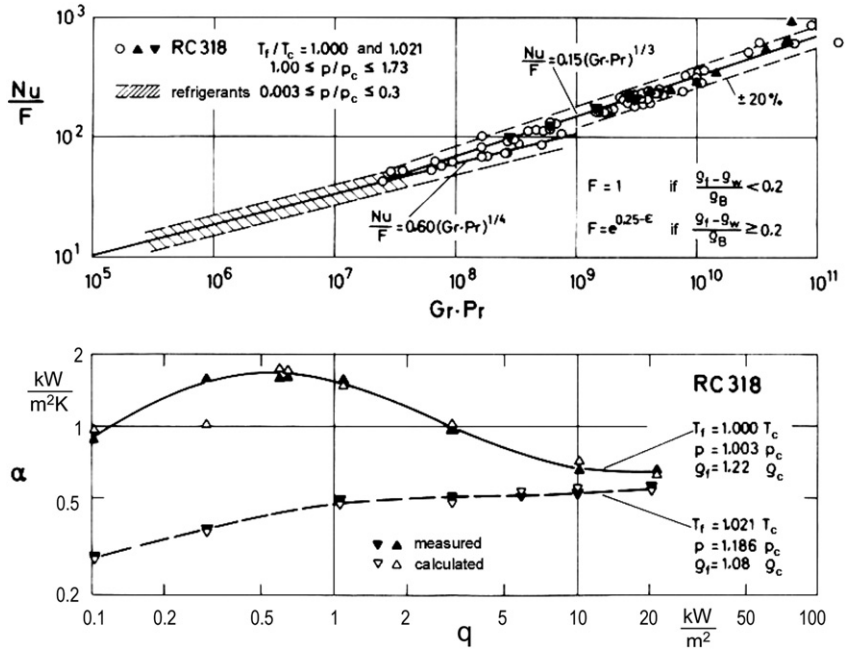

Fig. 19 – Earlier calculation method with modified *Nu* number *Nu/F* (from Solodov and Gorenflo, 1976).

B. Independent of the improvement under *A*., the interpolation lines for ΔT = const in the lowest diagram are shifted to higher α-values for higher ΔT as is known from far sub-critical free convection (cf. e.g. the *Nu*-lines in Fig. 3 or 14). For $T_f = T_c$, however, this holds only for fluid states with $v_f > 1.25 v_c$ or $\rho_f < 0.8\rho_c$ (right-hand side of the intermediate diagram), while the opposite occurs near CP, i.e. higher α-values for *smaller* ΔT, in the same way as for film boiling (and $\Delta T < 100$–200 K) shown previously in Fig. 14. Only for $\rho^* > 1.5$ or $v^* < 2/3$, it is reverse again (intermediate diagram, on the left).

5.3. *Calculation of heat transfer*

For the calculation of *Nu* number from *Gr* and *Pr* numbers, the last two parameters were modified in Solodov and Gorenflo (1976) to

$$Gr \equiv \left(\frac{gD^3\rho_B}{\eta_B^2}\right)\cdot\left(\frac{\delta\rho}{\delta T}\right)_p \cdot \Delta T_{fw} = \left(\frac{gD^3\rho_B}{\eta_B^2}\right)\cdot\Delta\rho_{fw}, \tag{17a}$$

$$Pr \equiv \frac{\eta_B c_{pB}}{\lambda_B} = \left(\frac{\eta_B}{\lambda_B}\right)\cdot\left(\frac{\delta h}{\delta T}\right)_p = \left(\frac{\eta_B}{\lambda_B}\right)\left(\frac{\Delta h}{\Delta T}\right)_{fw} \tag{17b}$$

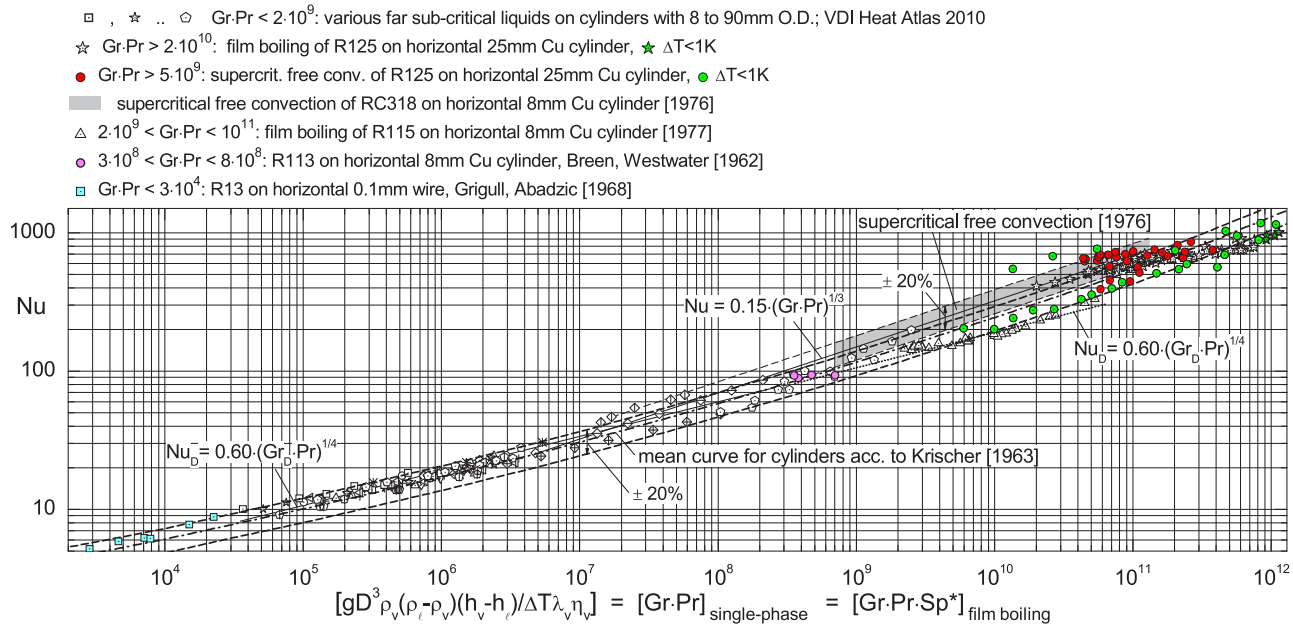

Fig. 20 – *Nu* (*Gr*,*Pr*)-representation of single-phase and two-phase free convection. New experimental data for R125/25 mm compared with earlier measurements for various fluids and cylinders and with calculation methods.

so $Nu = f(Gr{\cdot}Pr)$ is ending up in the generalized form of Eq. (15a),

$$Nu \equiv \frac{\alpha D}{\lambda_B} = f\left[\left(\frac{gD^3\rho_B}{\eta_B\lambda_B}\right)\cdot\left(\frac{\Delta h\Delta\rho}{\Delta T}\right)_{fw}\right] \quad (15b)$$

with the arithmetic mean temperature T_B of the fluid in the superheated boundary layer to be used for the three thermophysical properties of the fluid, and the three differences to be taken across the entire boundary layer from the fluid in the pool to the surface of the heated wall.

These definitions have been chosen because taking the differential terms in Eqs. (17a,b) at a fixed reference temperature may not be representative of their variation over the entire boundary layer near CP, as has been shown above, particularly in the diagrams of Fig. 17.

In the case of film boiling, the product of Pr number with the dimensionless ratio $Sp^* = \Delta h_{fw}/(c_p{\cdot}\Delta T_{fw})$ or

$$Pr{\cdot}Sp^* = \frac{\eta_B c_{pB}}{\lambda_B}\cdot\frac{\Delta h_{fw}}{c_p\Delta T_{fw}} = \frac{\eta_B}{\lambda_B}\cdot\left(\frac{\Delta h}{\Delta T}\right)_{fw} \quad (17c)$$

has to be taken to get Eqs. (15a,b).

Resulting from the earlier measurements, a slight modification in the calculation of Nu according to Eq. (15b) was proposed (Solodov and Gorenflo, 1976), if the relative variation of density across the superheated boundary layer exceeds 20%, with Nu in the generalized form of Eq. (15b) – or the specific forms of Eqs. (2a) and (2b) – to be replaced by Nu/F and $F = e^{0.25\,-\,\varepsilon}$ as given in Fig. 19, top.

Density at arithmetic mean temperature $T_B = (T_w - T_f)/2$ is used as reference value ρ_B, and parameter $\varepsilon = (\rho_B - \rho_w)/(\rho_f - \rho_w)$ characterizes the asymmetry of density variation across the boundary layer. It can be seen from a run with a maximum in the $\alpha(q)$-dependence, added as an example in the lower diagram, that also this feature is represented quite well by the modification.

The upper diagram demonstrates that the experimental scatter for (almost) all the earlier results for RC318 and an 8 mm tube (from Bier et al., 1976) in near-critical free convection remains within the limits of ±20% that had been found earlier for far sub-critical free convection of many fluids. In Fig. 20, the data of RC318 are shown as a shaded area and compared with the new measurements of R125 and the 25 mm tube for supercritical free convection and film boiling and with film boiling of R115, R113 on 8 mm tubes and R13 on a thin wire, and also with the data in the updated VDI-Heat Atlas (Gorenflo and Kenning, 2010) for far sub-critical measurements with many fluids and tubes with 8 to about 90 mm O.D.

The following conclusions can be drawn from Fig. 20:

A) The data cover wide ranges of Nu number ($5 < Nu < 1200$) and the product $Gr{\cdot}Pr$ ($2000 < Gr{\cdot}Pr < 1.2 \times 10^{12}$) and follow the trend of the so-called **mean curve for cylinders** according to Krischer (dot-dashed; Krischer, 1963) throughout the entire variation of $Gr{\cdot}Pr$.

B) For $Gr{\cdot}Pr < 10^9$, Eq. (2a) agrees with the <mean curve> within about ±10% and the scatter of the data for **far sub-critical free convection** remains within ±20%, except for a few data points that deviate by about +20% *from* Eq. (2b).

C) Near-critical **film boiling** of R13 on a thin wire and far sub-critical film boiling of R113 on an 8 mm cylinder agree well with both, the mean curve and Eq. (2a), and the latter represents also the film boiling data of R115 very well up to $Gr{\cdot}Pr = 5 \times 10^{10}$, whereas the data < jump > on the mean curve for the last few points with $Gr{\cdot}Pr \geq 7 \times 10^{10}$ indicating the onset of turbulent behaviour of the vapour film.

Film boiling on the 25 mm cylinder starts within the shaded area for supercritical free convection on the 8 mm cylinder, both following the trend of Eq. (2b) for turbulent boundary layer, but with increasing product of $Gr{\cdot}Pr$, the new data drift toward the lower limit of scatter for the mean curve and slightly beyond it.

D) **Supercritical free convection** for the 8 mm cylinder is well represented by Eq. (2b), if Nu is modified by the factor F where appropriate. For the 25 mm cylinder, the data follow the trend analyzed above for film boiling, but with higher scatter. A closer look at the data reveals that most of the data points for small superheats $\Delta T < 1$ K agree well with the dashed lower limit of scatter for the mean curve (and those for small $Gr{\cdot}Pr$ with Eq. (2a)). Also (the only) four near-critical points for film boiling with $\Delta T < 1$ K (and $p^* \geq 0.98$) at the end of the $Gr{\cdot}Pr$-scale lie close to the lower dashed curve.

Similar agreement of Nu numbers between near-critical film boiling and supercritical free convection at $p^* = 1.08$ with maximum deviations below 15% have been found in (Berthoud and Gros D'Aillon, 2009) for water and a thin wire as heating element.

The superheats of the three data points within $10^{10} < Gr{\cdot}Pr < 6 \times 10^{10}$ deviating most to *higher* Nu numbers are very small (19, 32, 52 mK) so this deviation might be caused by bigger *relative* errors in the ΔT-measurement. On the other hand, the fluid state ($T^* = 1.001$, $p^* = 1.008$) is very close to CP so the state of the entire (isobaric) superheated boundary layer is closer to CP than the pool, as can be seen in the lower diagrams of Fig. 16 – so the deviations might also be caused by large and asymmetrical variation of thermophysical properties, and T_B might not be appropriate as reference temperature.

A new calculation method including the particular variation of properties near CP and replacing the previous modification by the factor F has not been tried. By using the calculation methods that have been highly improved since 1976 and the much better knowledge of near-critical variation of thermophysical properties, it is very likely that the scatter of the new supercritical data will be reduced significantly, if the property variation within the superheated boundary layer is included in the determination of experimental Nu numbers, so the data can provide a better base for improving the prediction of heat transfer in the future.

6. Conclusions

For *nucleate boiling*, the updated VDI-Heat Atlas calculation method based on the Principle of Corresponding States predicts the new measurements very well at reduced pressures $p^* \leq 0.35$ at all heat fluxes and at low values of q for

higher p^*, up to its upper border of validity ($p^* = 0.9$). Increasing deviations of the experimental results towards higher values of α at $p^* \geq 0.65$ above a threshold value of q that decreases with increasing p^* may be caused by the particular roughness pattern produced by double sandblasting of the heated surface, with many tiny cavities of similar size and shape that are effective as active nucleation sites under these conditions. The deviations demonstrate again that the influences of surface roughness (and other properties of the heated wall) are not represented as well as other parameters in the prediction methods of nucleate boiling heat transfer.

Established expressions for the relative dependence on p^* of the *critical heat fluxes* q_{max} *and* q_{min} for transitions between nucleate and film boiling require adjustment to lower values for p^* close to the Critical Point. For $p^* > 0.93$, the decrease in $q_{min}/q_{min,0.1}$ for R125 on a 25 mm tube is smaller than for previous measurements for other fluids on 8 mm tubes. Photographic evidence suggests this is due to wavy disturbances of the vapour film.

The new data for heat transfer in *film boiling and supercritical free convection* very close to the Critical Point lead to a unified treatment covering the entire range from low sub-critical values of p^* to supercritical values $p^* \sim 1.75$.

Acknowledgements

The authors are grateful to Andrea Luke for all roughness measurements and evaluations, to Danijel Ninkovic for his assistance in the experiments, to Deutsche Forschungsgemeinschaft (DFG) for funding most of the experimental equipment, and last but not least, to Solvay Fluor und Derivate GmbH for supplying the refrigerant.

REFERENCES

Alpay, H.E., Gorenflo, D., 1983. Burnout heat transfer to SF6/R13B1- mixtures at near-critical saturation pressures. In: Proc. 16th Int. Congress of Refrigeration, Paris, vol. 2, pp. 155–162.

Baumhögger, E., Buljina, I., Gorenflo, D., 2008. Wärmeübergang beim Sieden von R 125($CHF_2.CF_3$) in freier Konvektion bis in den kritischen Zustandsbereich. DKV-Tagungsbericht, Bd.II.I, pp. 127–153.

Berthoud, G., Gros D'Aillon, L., 2009. Film boiling heat transfer around a very high temperature thin wire immersed into water at pressure from 1 to 210 bar: experimental results and analysis. Int. J. Therm. Sci. 48, 1728–1740.

Bier, K., Engelhorn, H.R., Gorenflo, D., Solodov, A.P., 1976. Wärmeübergang bei einphasiger freier Konvektion in der Nähe des kritischen Zustandes. Wärme- und Stoffübertragung 9, 193–202.

Bier, K., Gorenflo, D., Wickenhäuser, G., 1977a. Pool boiling heat transfer at saturation pressures up to critical. In: Hahne, E., Grigull, U. (Eds.), Heat Transfer in Boiling. Hemisphere Publishing Corporation, Washington, London, pp. 137–158.

Bier, K., Engelhorn, H.R., Gorenflo, D., 1977b. Heat transfer at burnout and Leidenfrost points for pressures up to critical. In: Hahne, E., Grigull, U. (Eds.), Heat Transfer in Boiling. Hemisphere Publishing Corporation, Washington, London, pp. 85–98.

Borishanskij, V.M., 1969. Correlation of the effect of pressure on the critical heat flux and heat transfer rates using the theory of thermodynamic similarity. In: Kutateladze, S.S. (Ed.), Problems of Heat Transfer and Hydraulics of Two-phase Media. Pergamon Press, Oxford, pp. 16–37.

Breen, B.P., Westwater, J.W., 1962. Effect of diameter of horizontal tubes on film boiling heat transfer. Chem. Eng. Progr. 58, 67–72.

Bromley, L.A., 1950. Heat transfer in stable film boiling. Chem. Eng. Progr. 46, 221–227.

Bromley, L.A., 1952. Effect of heat capacity of condensate. Ind. Eng. Chem. 44, 2966–2969.

Cichelli, M.T., Bonilla, C.F., 1945. Heat transfer to liquids boiling under pressure. Trans. AIChE 45, 755.

Gorenflo, D., 1977. Wärmeübergang bei Blasensieden, Filmsieden und einphasiger freier Konvektion in einem grossen Druckbereich, Abh. Deutsch. Kälte- u. Klimatechn. Verein Nr. 22. C.F.Müller-Verlag, Karlsruhe.

Gorenflo, D., 1982. Stand der Berechnungsmethoden zum Wärmeübergang bei der Verdampfung von Kältemitteln in freier Konvektion. DKV-Tagungsbericht 9, Essen, pp. 213–240.

Gorenflo, D., Baumhögger, E., Herres, G., 2009. Natural convective heat transfer near the critical state. Proc. 3rd IIR Conf. on Thermophysical Properties and Transfer Processes of Refrigerants, Boulder, CO, paper # 193.

Gorenflo, D., Kenning, D.B.R., 2010. Pool boiling. (Chapter H2). In: VDI Heat Atlas. Springer-Verlag, Berlin, Heidelberg.

Grigull, U., Abadzic, E., 1968. Heat transfer from a wire in the critical region. Proc. Inst. Mech. Engrs. 182 (Pt31), 52–57.

Haramura, Y., 1999. Critical heat flux in pool boiling. Chapter 6. In: Kandlikar, S.G., Shoji, M., Dhir, V.K. (Eds.), Handbook of Phase Change; Boiling and Condensation. Taylor and Francis, Philadelphia.

Hesse, G., 1972. Wärmeübergang bei Blasenverdampfung, bei maximaler Wärmestromdichte und im Übergangsbereich zur Filmverdampfung. PhD thesis, Techn. Univ. Berlin.

Hesse, G., 1973. Heat transfer in nucleate boiling, maximum heat flux and transition boiling. Int. J. Heat Mass Transf. 16, 1611–1627.

Hu, H.-P., Wang, C.-C., Chen, C.-K., 2008. Turbulent film boiling on a horizontal tube with variable wall temperature. Int. Comm. Heat Mass Tran. 35, 974–979.

Kang, D.G., Park, K.-J., Jung, D., 2009. Nucleate boiling heat transfer coefficients of halogenated refrigerants up to critical heat fluxes. In: Proc. 3rd IIR Conf. on Thermophysical Properties and Transfer Processes of Refrigerants, Boulder, CO., paper # 195.

Kotthoff, S., Gorenflo, D., 2009. Heat transfer and bubble formation on horizontal copper tubes with different diameters and roughness structures. Heat Mass Transf. 45, 893–908.

Krischer, O., 1963. Die wissenschaftlichen Grundlagen der Trocknungstechnik, 2nd ed. Springer-Verlag, Berlin.

Kutateladze, S.S., 1952. Heat transfer in condensation and in boiling. USAEC Rept. AECU-3770.

Kutateladze, S.S., 1963. Fundamentals of Heat Transfer. Academic Press.

Labuntsov, D.A., Jagov, V.V., Gorodov, A.K., 1978. Critical heat fluxes in boiling at low pressure region. In: Proc. 6th Int. Heat Transfer Conf., Toronto, vol. I, pp. 221–225.

Lienhard, J.H., Wong, P.T.Y., 1964. The dominant unstable wavelength and minimum heat flux during film boiling on a horizontal cylinder. J. Heat Transf. 86, 220–226.

Mostinskij, I.L., 1963. Application of the principle of corresponding states for calculation of heat transfer and critical heat flux of boiling liquids. Teploenergetica 10 (4), 66–71.

Nishio, S., 1999. Film boiling. In: Nishio, S., Auracher, H., Film and Transition Boiling. Chapter 7 of Handbook of Phase Change; Boiling and Condensation, Eds. Kandlikar, S.G., Shoji, M., Dhir, V.K., Taylor, Francis, Philadelphia.

Nishio, S., 1999. Film boiling. In: Nishio, S., Auracher, H. Film and Transition Boiling. Chapter 7 of Handbook of Phase Change; Boiling and Condensation, (Eds). Kandlikar, S.G., Shoji, M., Dhir, V.K. Taylor and Francis, Philadelphia.

Noyes, R.C., 1963. An experimental study of sodium pool boiling heat transfer. J. Heat Transf. 85, 125–131.

Sakurai, A., Shiotsu, M., Hata, K., 1990. A general correlation for pool film boiling heat transfer from a horizontal cylinder to subcooled liquid. Part 2: experimental data for various liquids and its correlation. J. Heat Transf. 112, 441–450.

Sarma, P.K., Dharma Rao, V., Bergles, A.E., 1997. Turbulent film boiling on a horizontal cylinder – effect of temperature dependent properties. Energy Convers. Manage. 38, 1135–1144.

Schömann, H., 1994. Beitrag zum Einfluss der Heizflächenrauhigkeit auf den Wärmeübergang beim Blasensieden. PhD thesis, University (GH) of Paderborn.

Sciance, C.T., Colver, C.P., Sliepcevich, C.M., 1967a. Pool boiling of methane between atmospheric pressure and the critical pressure. Adv.Cryog. Eng. 12, 395–408.

Sciance, C.T., Colver, C.P., Sliepcevich, C.M., 1967b. Nucleate pool boiling and burnout of liquefied hydrocarbon gases. Chem. Eng. Progr. Symp. Ser. 63 (77), 109–114.

Solodov, A.P., Gorenflo, D., 1976. Zur Berechnung des Wärmeübergangs bei einphasiger freier Konvektion in der Nähe des kritischen Zustandes. Wärme- und Stoffübertragung 9, 151–158.

Son, G., Dhir, V.K., 2008. Three-dimensional simulation of saturated film boiling on a horizontal cylinder. Int. J. Heat Mass Transf. 51, 1156–1167.

Stephan, K., 1963. Beitrag zur Thermodynamik des Wärmeübergangs beim Sieden. Abh. Deutsch. Kältetech. Ver. Nr. 18. Karlsruhe: Verlag C.F.Müller; cf. also: Chem Ing Techn 35, pp. 775–784.

Wickenhäuser, G., 1972. Einfluss der Wärmestromdichte und des Siededrucks auf den Wärmeübergang beim Blasensieden von Kältemitteln. PhD thesis, Univ. of Karlsruhe (TH).

Wright, R.D., Colver, C.P., 1969. Saturated pool boiling burnout of ethane-ethylene-mixtures. Chem. Eng. Progr. Symp. Ser. 65, 204–210.

Zuber, N., 1958. On the stability of boiling heat transfer. J. Heat Transf. 80, 711.

Zuber, N., Tribus, M., Westwater, J.W., 1961. Hydrodynamic crisis in pool boiling of saturated and subcooled liquids. In: Proc. Int. Heat Transfer Conf., Boulder, CO, paper # 27, pp. 230–236.

Zuber, N., 1968. In: Clark, J.A. (Ed.), Cryogenic Heat Transfer. Adv. in Heat Transfer 5. Acad. Press, New York, p. 325.